- Article type: paper (6200 words with 22 illustrations).
- 04/06/2015.
- 6200, 22 figures.

A numerical investigation of the incremental behavior of crushable granular soils

Author 1

Matteo Oryem Ciantia

Departamiento de Ingeniería del Terreno, UPC, Barcelona, Spain

Author 2

Marcos Arroyo

Departamiento de Ingeniería del Terreno, UPC, Barcelona, Spain

Author 3

Francesco Calvetti

Dipartimento di Igegneria Civile ed Ambientale (DICA), Politecnico di Milano,Italy

Author 4

Antonio Gens

Departamiento de Ingeniería del Terreno, UPC, Barcelona, Spain

Corresponding author contact: matteo.ciantia@upc.edu

Abstract

The mechanical behavior of granular materials is characterized by strong non-linearity and irreversibility. These properties have been differently described by a variety of constitutive models. To test any constitutive model, experimental data relative to the nature of the incremental stress-strain response of the material is desirable. However this type of laboratory data is scarce because of being expensive and difficult to obtain. The discrete element method has been used several times as an alternative to obtain incremental responses of granular materials. Crushable grains add one extra source of irreversibility to granular materials. Crushability has been variously incorporated into different constitutive models. Again, it will be helpful to obtain incremental responses of crushable granular materials to test these models, but the experimental difficulties are increased. Making use of a recently introduced crushing model for discrete element simulation, this paper presents a new procedure to obtain incremental responses in discrete analogues of granular crushable materials. The parallel probe approach, previously used for uncrushable discrete analogues, is here extended to account for the presence of crushable grains. The contribution of grain crushing to the incremental irreversible strain is identified and separately measured. Robustness of the proposed method is examined in detail, paying particular attention to aspects such as dynamic instability or crushing localization. The proposed procedure is later applied to map incremental responses of a discrete analogue of Fontainebleau sand on the triaxial plane. The effect of stress ratio and granular state on plastic flow characteristics is highlighted.

Keywords

Discrete element method, granular materials, incremental non linearity, crushing.

List of notation

F	is the contact force
$\sigma_{\lim}$	is the limit strength of the material
R	is the particle radius and
θ_0	is the contact angle defining the contact area
A_F	is the contact area
$\sigma_{\lim 0}$	is the mean limit strength of the material
d	is the particle diameter
d_0	is the reference particle diameter
m	is the Weibull modulus
k_N	is the normal contact stiffness
k_S	is the shear contact stiffness
G	is the particle shear modulus
ν	is the particle Poisson ratio

$\Delta\varepsilon$	is the total strain increment
$\Delta\varepsilon^{e}$	is the elastic strain increment
$\Delta\varepsilon^{pu}$	is the plastic -uncrushable strain increment
$\Delta\varepsilon^{pc}$	is the crush induced plastic strain increment
$\Delta\varepsilon^{ep}$	is the elasto-plastic strain increment
$\alpha_{\Delta\sigma}$	is the stress probe direction
$\Delta\sigma_{z}$	is the stress increment in the z direction
$\Delta\sigma_{r}$	is the stress increment in the r direction
$\alpha_{\Delta\varepsilon}$	is the direction of total strain increment
$\alpha_{\Delta\varepsilon}^{pu}$	is the direction of plastic strain increment
$\alpha_{\Delta\varepsilon}^{pc}$	is the direction of crush strain increment

1 Introduction

Grain fragmentation is significant for several important geotechnical problems, such as side friction on driven piles (Yang et al. 2010) or railway ballast durability (Indraratna et al. 2011). This has driven many efforts, both to incorporate grain crushing into constitutive models for soils (e.g. Cecconi et al. 2002; Muir Wood, 2007; Einav, 2007; Daouadji & Hicher, 2010; Liu et al. 2013) and to model soil crushing using DEM (Cheng et al. 2004; McDowell & DeBono, 2013; Ciantia et al. 2015). As it happens in other areas of geomechanics (e.g. Jiang et al 2007) these efforts are best seen as complementary. For instance, DEM models can provide ancillary experiments to supplement expensive and/or difficult laboratory tests.

This is the case of studies of the incremental response of granular materials. By incremental response is understood the deformation responses to a series of "small" incremental solicitations (probes) that, starting from a unique initial state, point towards various directions in the stress space. The incremental response (Gudehus, 1979; Tamagnini et al. 2000; Darve & Nicot, 2005; Froiio & Roux, 2010) is a powerful tool for the verification of basic constitutive postulates – existence and characteristics of incremental nonlinearity, associative behaviour, uniqueness of flow rule, etc.

Obtaining incremental responses in the laboratory is possible, (Constanzo et al. 2006), but difficult because of the tight control in terms of strain measurements that is required and because of the need for testing several identical samples (one for each probe). For this reason DEM models have been used to study the incremental behavior of granular materials, first in 2D (Bardet, 1994, Calvetti & di Prisco 1993) and later in 3D (Calvetti et al 2003; Tamagnini et al 2005; Plassiard et al 2009; Thornton & Zhang 2010; Wan & Pinheiro, 2013). None of these previous studies of incremental responses using DEM has considered the case of crushable soils.

In this work the practice of stress probing using DEM is extended to cases where significant particle breakage is present. A DEM model calibrated to represent Fontaineblau sand is incrementally tested exploring a variety of initial state conditions within the triaxial plane. To do so it is first necessary to introduce the basic features of the discrete modelling approach here employed. Next, the procedure followed to obtain an incremental strain response is described, indicating how such response can be decomposed in three different contributions: elastic, plastic-unbreakable and plastic-crushing. Section 4 presents the first numerical results, obtained in oedometric conditions. These results are used to clarify a number of important computational aspects of the proposed procedure: selection of an appropriate representative volumetric element (REV); characteristics of spatio-temporal crushing patterns; effect of some discrete model hypothesis. Finally, in section 5 the method is systematically applied to explore the effect

of stress obliquity and grading index on the plastic flow pattern on triaxial conditions. A few conclusions follow to encourage further applications of the proposed method.

2 Discrete model

Recently (Ciantia et al. 2014, 2015), the authors have proposed and tested a crushable soil DEM modelling approach that, while biased towards effective computation, showed good ability to reproduce macroscopic responses of a variety of soils. In this section the main traits of that approach are briefly outlined. All models are built using the PFC3D code (Itasca, 2008).

2.1 Particle failure criteria

The failure criteria used in the model was inspired by Russell and Wood, 2009a and Russell et. al, 2009b. The authors combined a two-parameter material strength criterion with the analysis of the elastic stress distribution induced by point loads on a sphere to obtain a failure criterion. Without entering into the details of the mathematical formulation, the end result of their analysis can be summarized as follows: a particle subject to a set of external point forces will reach failure when the maximum acting force reaches the following limit condition:

$$F \leq \sigma_{\lim} \pi R^2 \sin^2 \theta_0 = \sigma_{\lim} A_F \tag{1}$$

where $\sigma_{\lim}$ is the limit strength of the material, R is the particle radius and θ_0 the contact angle defining the contact area. As indicated, the limiting force is obtained as the product of a limit strength value, $\sigma_{\lim}$, dependent on material parameters, and a contact area A_F.

To incorporate within-size variability into the simulation, the limit strength, $\sigma_{\lim}$, is assumed as normally distributed for a given sphere size, with a mean value indicated as $\sigma_{\lim 0}$ and coefficient of variation, *var*. A size effect correction is also incorporated as a dependency of the mean strength value on particle diameter:

$$\sigma_{\lim} = \sigma_{\lim,0} \left(\frac{d}{d_0} \right)^{-3/m} \tag{2}$$

2.2 Contact law

In this work the contact law is the simplified Hertz-Mindlin one, and the standard formulation (Itasca, 2008) is used. The normal and shear stiffness are calculated as:

$$k_N = \left(\frac{2\langle G \rangle \sqrt{2 \frac{D_1 D_2}{D_1 + D_2}}}{3\left(1 - \langle \nu \rangle\right)} \right) \sqrt{U} \tag{3}$$

$$k_S = \left(\frac{2\left(\langle G \rangle^2 3\left(1-\langle \nu \rangle\right) \frac{D_1 D_2}{D_1 + D_2} \right)^{1/3}}{2-\langle \nu \rangle} \right) |F|^{1/3} \tag{4}$$

where U is the sphere overlap, F is the magnitude of the normal contact force and the $\langle\ \rangle$ brackets indicate the mean value of the quantity considered of the two balls in contact (shear modulus G and Poisson ratio ν).

To evaluate the contact area A_F in (1) Hertzian contact theory is also applied. For smooth spheres the radius of the contact area is:

$$r_H = \left(\frac{3Fr'}{4E'} \right)^{1/3} \tag{5}$$

where

$$r' = \left(\frac{1}{r_1} + \frac{1}{r_2} \right)^{-1} \tag{6}$$

$$E' = \left(\frac{1-\nu_1^2}{E_1} + \frac{1-\nu_2^2}{E_2} \right)^{-1} \tag{7}$$

where r_1 and r_2 are the radius of the contacting spheres and E_1, v_1 their moduli.

2.3 Particle splitting configuration

Once the limit condition is reached, a particle, modeled as a sphere in PFC, will split into smaller inscribed tangent spheres. The daughter fragments assume the velocity and material parameters of the mother particle except for the intrinsic strength ($\sigma_{\lim 0}$) that is randomly assigned in accordance with the normal distribution criteria.

Ciantia et al (2015) compared alternative splitting configurations, concluding that the 14-ball crushed configuration represented in Figure 1 is accurate enough to represent macroscopic behavior. The same splitting configuration has been adopted here for incremental probing. The particle split proposed implies some mass loss. The influence of this assumption on the proposed procedure is discussed below in section 4.

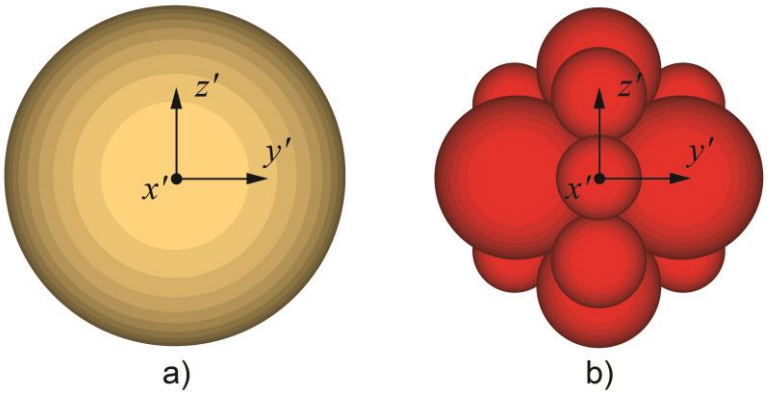

Figure 1 a) Initial particle, b) Particle splitting configuration.

2.4 Grading and grading index

The particle mass not retained into the discrete model is accounted for in postprocessing. Thus, particle mass deleted upon breakage is assumed to distribute in particles smaller than those begotten by the particle split, fitting a limiting size distribution, which is assumed fractal (see Ciantia et al. 2015, for details). At every instant the size distribution of the particles retained in the discrete model is complemented by the distribution assumed for those excluded. This allows tracking the evolving grain size distribution (GSD) of a test specimen on a certain loading path.

An evolving GSD can be described in a number of ways. In this work we will sometimes present directly the evolved GSD, but to achieve a more compact discussion we would also follow the proposal of Muir Wood (2007), who introduced a grading state index, I_G. As illustrated in Figure 2, I_G can be computed as the area ratio of the current grading, to the limiting grading.

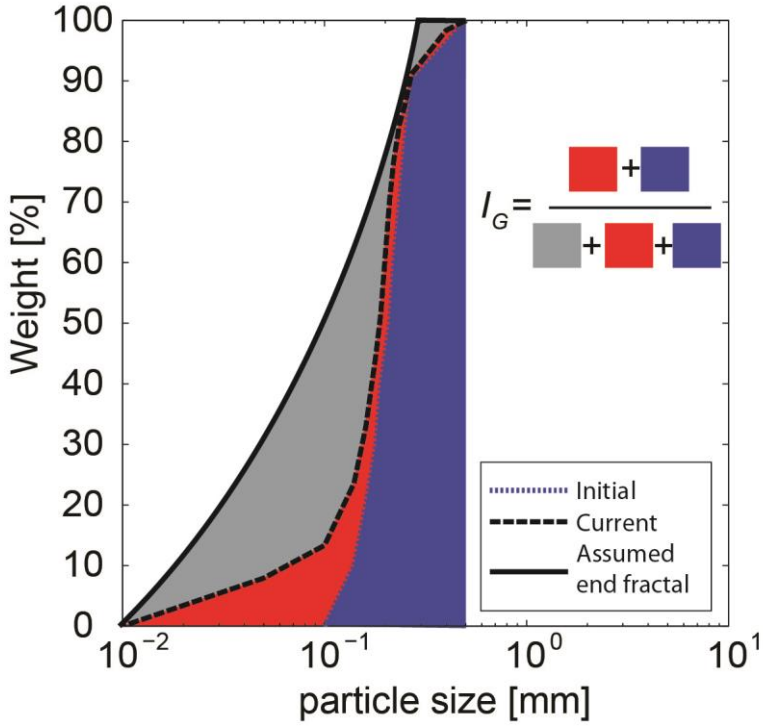

Figure 2 Muir Wood (2007) grading state index

3 Incremental strain response: methods

3.1 Stress probes

In the particular case of axisymmetric (triaxial) loading, the number of independent stress and strain variables reduces to two, and a convenient graphical representation can be given in a Rendulic plane. In the Rendulic plane of stress increments see Figure 3a, the magnitude of stress probes is

$$\begin{aligned} \|\Delta\sigma\| &:= \sqrt{\Delta\sigma \cdot \Delta\sigma} = \sqrt{(\Delta\sigma_x)^2 + (\Delta\sigma_y)^2 + (\Delta\sigma_z)^2} = \sqrt{(\Delta\sigma_r)^2 + (\Delta\sigma_z)^2} \\ \Delta\sigma_r &= \sqrt{2}\Delta\sigma_x = \sqrt{2}\Delta\sigma_y \end{aligned} \tag{8}$$

and the stress probe direction is defined by the angle $\alpha_{\Delta\sigma}$ between the $\Delta\sigma_r$ axis and the stress increment vector:

$$\alpha_{\Delta\sigma} = \tan^{-1}\left(\frac{\Delta\sigma_z}{\Delta\sigma_r}\right) \quad \alpha_{\Delta\sigma} \in [0;360] \tag{9}$$

The magnitude of the stress probes in this study was typically selected as 1% of the initial mean stress.

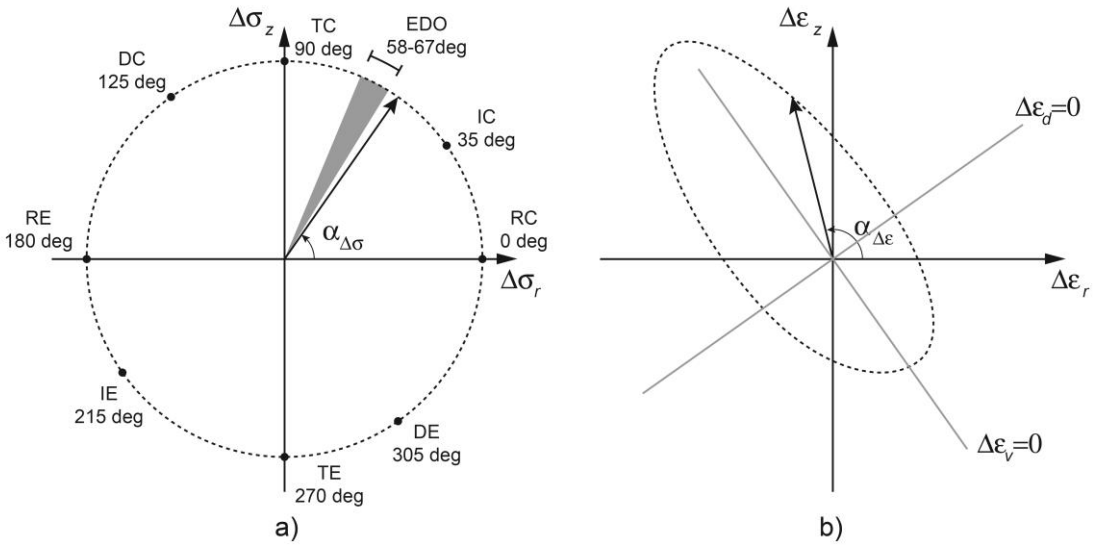

Figure 3 Stress probes: IC/E = isotropic compression/expansion, TC/E = "triaxial" (axi-symmetric) compression/extension; DC/E = purely deviatoric compression/extension; RE/C = radial extension/compression; EDO = oedometric compression within the range of k0 developed in the whole simulation. b) Representative response envelope to stress probes

The response is depicted by using the so-called *incremental strain response envelope* (Tamagnini *et al.* 2000a). This is plotted in a Rendulic plane for strain increments, ($\Delta\varepsilon_z : \Delta\varepsilon_r$) (Figure 3b). The direction of strain increment is defined by the angle $\alpha_{\Delta\varepsilon}$, between the $\Delta\varepsilon_r$ axis and the strain increment vector:

$$\alpha_{\Delta\varepsilon} = \tan^{-1}\left(\frac{\Delta\varepsilon_z}{\Delta\varepsilon_r}\right) \quad \alpha_{\Delta\varepsilon} \in [0;360] \tag{10}$$

In Figure 3b the strain increment directions corresponding to pure deviatoric and pure volumetric strain are also indicated for reference.

3.2 Strain response decomposition

For small strains and additive decomposition into reversible (or "elastic", used here as synonymous of reversible), $\Delta\varepsilon^e$, and irreversible (or "plastic") parts is appropriate:

$$\Delta\varepsilon = \Delta\varepsilon^e + \Delta\varepsilon^p \tag{11}$$

There are two possibilities to separate the reversible and irreversible parts using DEM. The first one is to reproduce the laboratory approach: a load-unload cycle is performed for each stress probe, the strain remaining after complete unloading is plastic; that recovered upon unloading is elastic. We will call this the load-unload approach.

Tamagnini et al (2005) proposed a different approach. To obtain the elastic strains an identical loading probe is performed on a different model, which was an elastic counterpart of the original DEM specimen. Such elastic counterpart was obtained by inhibiting all the mechanisms

responsible for plasticity before starting the probe. This was done by artificially raising contact friction so that contact sliding is impossible. Every other single aspect of the original model (i.e. particle arrangement and contact forces) is preserved. We will call this the parallel probe approach.

Wan & PInheiro (2013) explicitly compare the parallel probe and load-unload approach. Identical plastic strains were obtained and therefore the two approaches were deemed equivalent. Of course, they were always using uncrushable particles.

If particles are allowed to crush, the total incremental strain $\Delta\varepsilon$ can still be seen as the sum of elastic and plastic components. But the plastic strain has now two contributions, one that will appear even if all particles were unbreakable, which is here called “plastic-uncrushable” and noted $\Delta\varepsilon^{pu}$. Another is the extra plastic strain that appears due to particle crushing. These extra plastic strain increments induced by crushing are here noted $\Delta\varepsilon^{pc}$ and called “plastic-crushable”.

$$\Delta\varepsilon = \Delta\varepsilon^{e} + \Delta\varepsilon^{p} \qquad (12)$$

$$\Delta\varepsilon^{p} = \Delta\varepsilon^{pu} + \Delta\varepsilon^{pc} \qquad (13)$$

At this stage it is practical to introduce the concept of conventional elasto-plastic strain, $\Delta\varepsilon^{ep}$ which is the incremental strain that would be observed upon probing a DEM model in which particle breakage has been inhibited. It follows that

$$\Delta\varepsilon^{ep} = \Delta\varepsilon^{e} + \Delta\varepsilon^{pu} \qquad (14)$$

$$\Delta\varepsilon = \Delta\varepsilon^{ep} + \Delta\varepsilon^{pc} \qquad (15)$$

A generalization of the parallel probe approach is proposed to separate the elastic, plastic-uncrushable and plastic-crushable incremental strain contributions. Three tests are run in parallel for each stress probe.

1. The first one runs on a specimen described by the reference discrete model. It provides the total strain increment $\Delta\varepsilon$
2. The second one runs in a non-crushable counterpart of the original specimen, in which crushing is inhibited. It provides the conventional elasto-plastic strain increment $\Delta\varepsilon^{ep}$

3. The third one runs on an “elastic” counterpart of the DEM specimen, in which all the mechanisms responsible for plasticity (interparticle sliding and particle crushing) are inhibited. It provides the elastic strain increment $\Delta\varepsilon^{e}$

The two incremental plastic strain contributions are then obtained as follows

$$\Delta\varepsilon^{pu} = \Delta\varepsilon^{ep} - \Delta\varepsilon^{e} \tag{16}$$

$$\Delta\varepsilon^{pc} = \Delta\varepsilon - \Delta\varepsilon^{e} - \Delta\varepsilon^{pu} \tag{17}$$

The robustness of the proposed procedure for incremental strain decomposition is examined in the following section.

4 Incremental strain response: computational issues

4.1 A REV of Fontainebleau sand

A response envelope (RE) is obtained by repeatedly testing a representative volumetric element (REV) of the material under study. The DEM model of a REV should be as small as possible to ease computation, but large enough so that the response observed at the boundaries would not change with further size increases. Previous experience with uncrushable sands was not unanimous in this respect, with particle numbers in REV ranging from 3500 (Calvetti et al 2004) to 27000 (Thornton & Zhang, 2010). Here three different numerical specimens with side lengths of 3, 4 and 6 mm and filled with about 5000, 10000, and 35000 particles respectively (Figure 4) were initially explored.

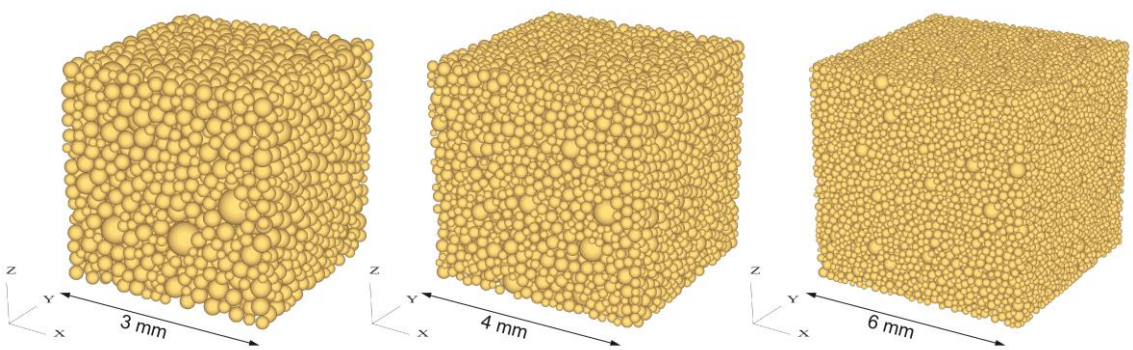

Figure 4. The three (small, mid, large) candidate DEM models for incremental testing, visualised with different magnification.

These cubic specimens are filled with randomly assembled weightless spherical particles. The grain size distribution corresponds closely to that of Fontainebleau sand (Yang et al. 2010) with

particle diameters ranging from 0.1 to 0.4 mm. Specimen boundaries are defined by introducing smooth “wall” elements, to which displacement rates can be imposed. Target stress values are applied using a servo-control to adjust wall displacement. The smooth rigid boundaries ensure that the principal axes of stress and strain are coincident with the cube axis. Principal strains are then calculated directly from wall displacements, while the corresponding principal stresses are obtained from boundary forces.

The large model was used for parameter calibration. Standard contact law parameters (G, v and ϕ) were calibrated using uncrushable particles to simulate the drained triaxial compression of a dense specimen under 100 kPa confinement (marked “Dr 0.7” in Figure 5a). A validation was performed using a similar test for a loose sample (“Dr 0.3” in Figure 5a). Parameters controlling particle failure (m, CV and σ_{lim0}) were initially estimated using fused silica material properties and single-particle crushing data for other sands. These estimates were later refined to match a one dimensional high pressure compression test (Fig3b). More details on calibration procedures for this crushable DEM approach can be found in Ciantia et al, (2014a and 2015); the calibrated parameters used here are summarized in Table 1.

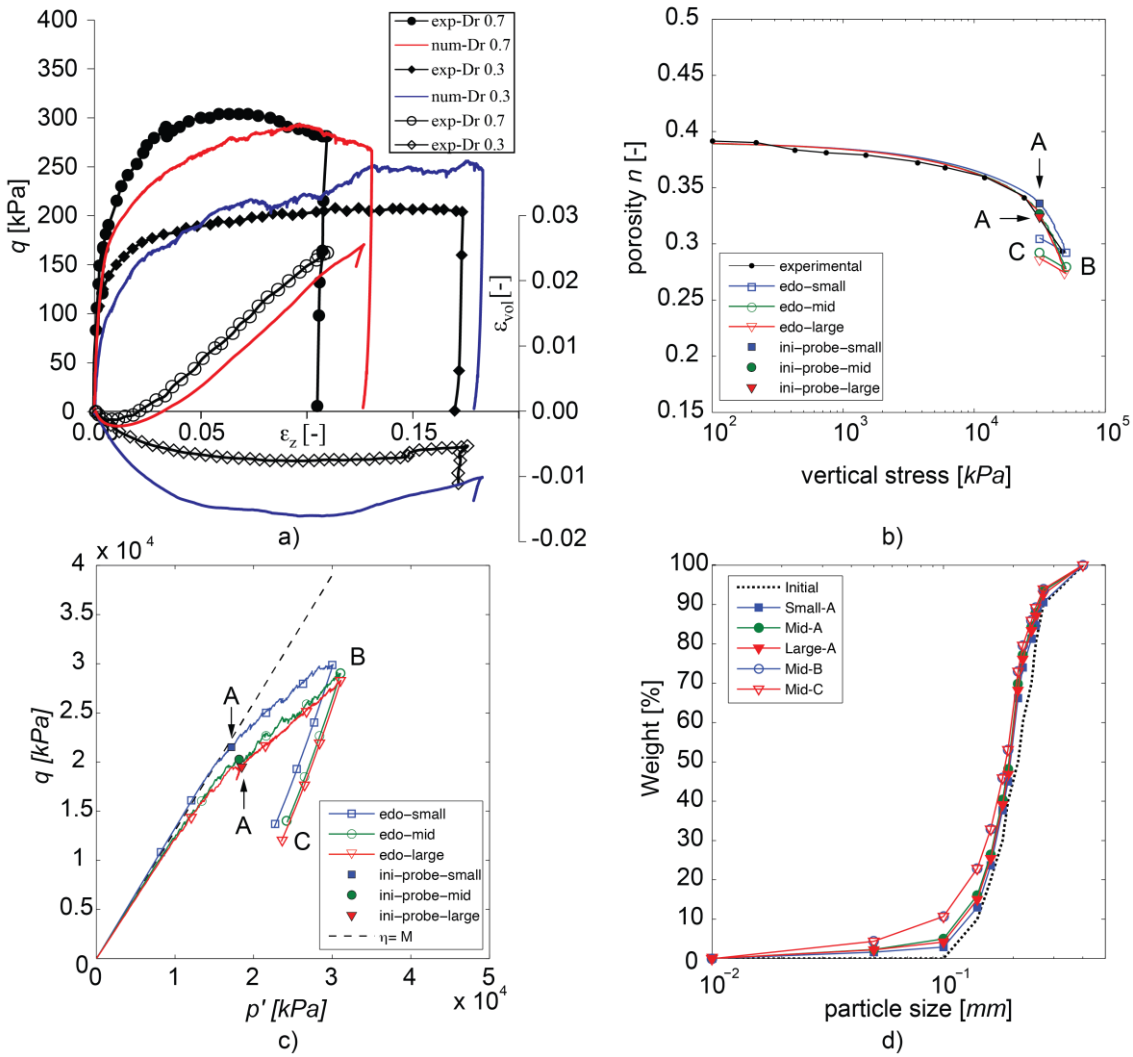

Figure 5 DEM-simulation of drained triaxial compression test (cell pressure 100 kPa) a) deviatoric stress vs axial strain and volumetric strain vs axial strain and b) oedometric compression and of Fontainebleau sand. Point A B and C represent three initial conditions for the stress probe analyses, c) stress paths for small, medium and large samples, d) GSD at point A for the three samples and for the mid sample at point B and point C.

Table 1 Discrete-element method input parameters for simulation

d_{50} [mm]	ϕ [rad]	G [kPa]	ν [–]	$\sigma_{lim,0}$ [kPa]	m	d_0 [mm]	CV
0.21	0.27	3e6	0.3	5e6	10	2	1

4.2 An example: incremental response at oedometric loading

The first initial state selected for probing was reached by one dimensional or oedometric compression up to σ_z = 31.5 MPa (point A in Figure 5b). Following (Cheng et al 2004) the apparent yield point of the loading curve can be taken as an indication that crushing had already started at this stage. Grain size distribution and fabric will change on crushing. A first judgement on the quality of the differently sized models can be obtained comparing their behavior up until this probing point.

At the reference stress level, the small-N specimen porosity is slightly above that of the experimental result. The medium and large-N specimens are almost coincident with the experiment. The differences in grain size distribution (Figure 5d) appear relatively small, but it is also apparent that the smaller specimen followed a different stress path, (Figure 5c) with lower K_0 than the other two. This (Ciantia et al, 2015) is indicative of smaller relative crushing and indeed the micromechanical variables reported in Table 2 confirm that impression. It was thus established that the small-N specimen was inadequate as REV.

Table 2 Initial conditions of the numerical samples

sample	*point*	N_0	N_A	*1st generation*	*2nd generation*	*3rd generation*	σ_z	σ_x	σ_y	*n*
small	A	4389	4675	4367	308	0	31.5	10.0	10.0	0.336
mid	A	10397	13231	10180	3037	14	31.5	11.1	11.3	0.319
large	A	35083	40361	34679	5654	28	31.5	12.0	12.0	0.324
mid	B	10397	21785	9583	11334	868	50	22	22	0.268
mid	C	10397	21785	9583	11334	868	31.5	20	20	0.281

Points B and C highlighted in Figure 5 refer to the initial state of the medium sample that has been loaded up to a vertical stress of 50 MPa and subsequently unloaded to the same vertical stress characterizing point A, respectively. In Table 2 the micromechanical variables at these two conditions are also reported. The incremental responses obtained at those points are discussed in section 5.1, for the moment we focus on the response obtained at point A using the large sample.

In Figure 6 the strain response envelopes obtained from stress probing at point A on the oedometric path is presented. The upper panel shows the strain response envelopes for the elastic, elasto-plastic and elasto-plastic-crushable case. The elastic envelope is symmetrical about the origin, whereas the envelopes in which plastic mechanisms are active are markedly asymmetric. Asymmetry of the strain envelope response indicates incremental non linearity. This first test suggests then that grain crushing increases the non-linearity of incremental response.

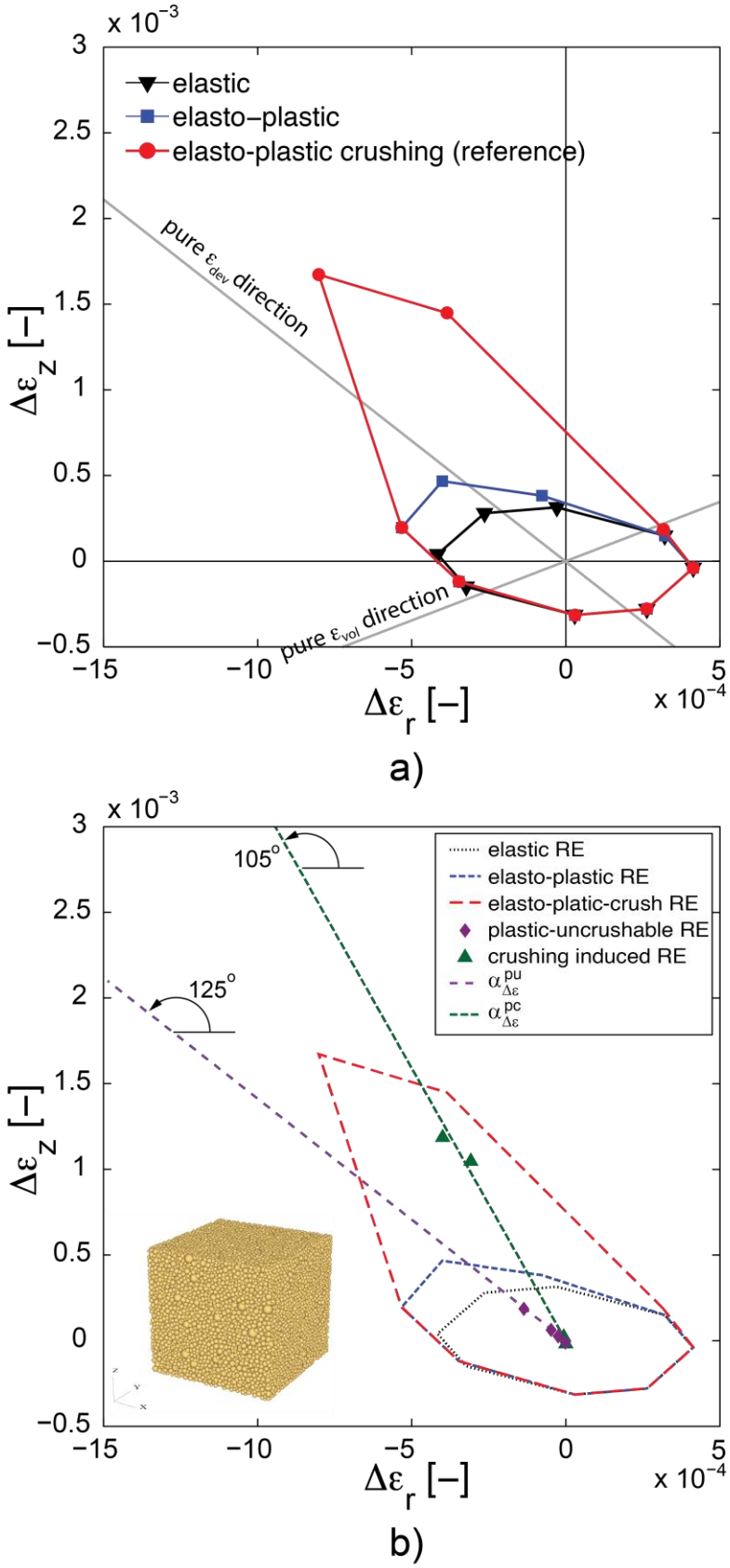

Figure 6. Elastic, elasto-plastic and elasto-plastic with crushing strain envelopes at point A on the oedometric loading path. a) elastic, elasto-plastic (uncrushable) and elasto-plastic-crushable strain envelopes. b) plastic and plastic-crushable incremental strains. All responses obtained obtained using the large specimen (shown in the inset)

The incremental plastic strain components are shown in Figure 6b. They lie very close to two different lines, which correspond to the direction of plastic flow due to crushing and that due to other mechanisms. Without crushing plastic flow is practically aligned with a purely deviatoric strain (see Figure 3 b). The crushing induced plastic strains are neither purely deviatoric nor purely volumetric, aligning at 105°. Because of their larger magnitude they dominate total plastic strain. Activating crushing induces more volumetric plastic strains and rotates the plastic flow direction away from the purely deviatoric case.

This is confirmed in more detail in Figure 7, where in the left column the magnitude of the total ($\Delta\varepsilon$), plastic-uncrushable ($\Delta\varepsilon^{pu}$), and plastic-crushable ($\Delta\varepsilon^{pc}$) strain increments is represented as a function of the loading direction, while in the right column the direction of total strain increments ($\alpha_{\Delta\varepsilon}$), plastic-uncrushable strain increment ($\alpha_{\Delta\varepsilon}^{pu}$), and plastic-crushable strain increment ($\alpha_{\Delta\varepsilon}^{pc}$), defined as

$$\alpha_{\Delta\varepsilon}^{pu} = \tan^{-1}\left(\frac{\Delta\varepsilon_z^{pu}}{\Delta\varepsilon_r^{pu}}\right) \quad \alpha_{\Delta\varepsilon}^{pu} \in [0;360] \quad \text{and} \quad \alpha_{\Delta\varepsilon}^{pc} = \tan^{-1}\left(\frac{\Delta\varepsilon_z^{pc}}{\Delta\varepsilon_r^{pc}}\right) \quad \alpha_{\Delta\varepsilon}^{pc} \in [0;360] \tag{18}$$

are plotted as a function of stress probe direction $\alpha_{\Delta\sigma}$. Following Calvetti et al (2003) a truncated cosine fit has been included in the figures to guide the eye. The response in some loading directions remains purely elastic, for instance in those around 250°, diametrically opposed to the ongoing oedometric path direction (Figure 3a). Plastic-crushable strains are larger but appear in fewer probes than plastic-uncrushable strains. Maximum plastic strains appear in the direction of pure deviatoric compression (DC Figure 3a) which is some 60° more deviatoric than the ongoing oedometric path. Interestingly, the plastic strain direction is fixed for each mechanism, but it does vary when the two separate plastic mechanisms are combined.

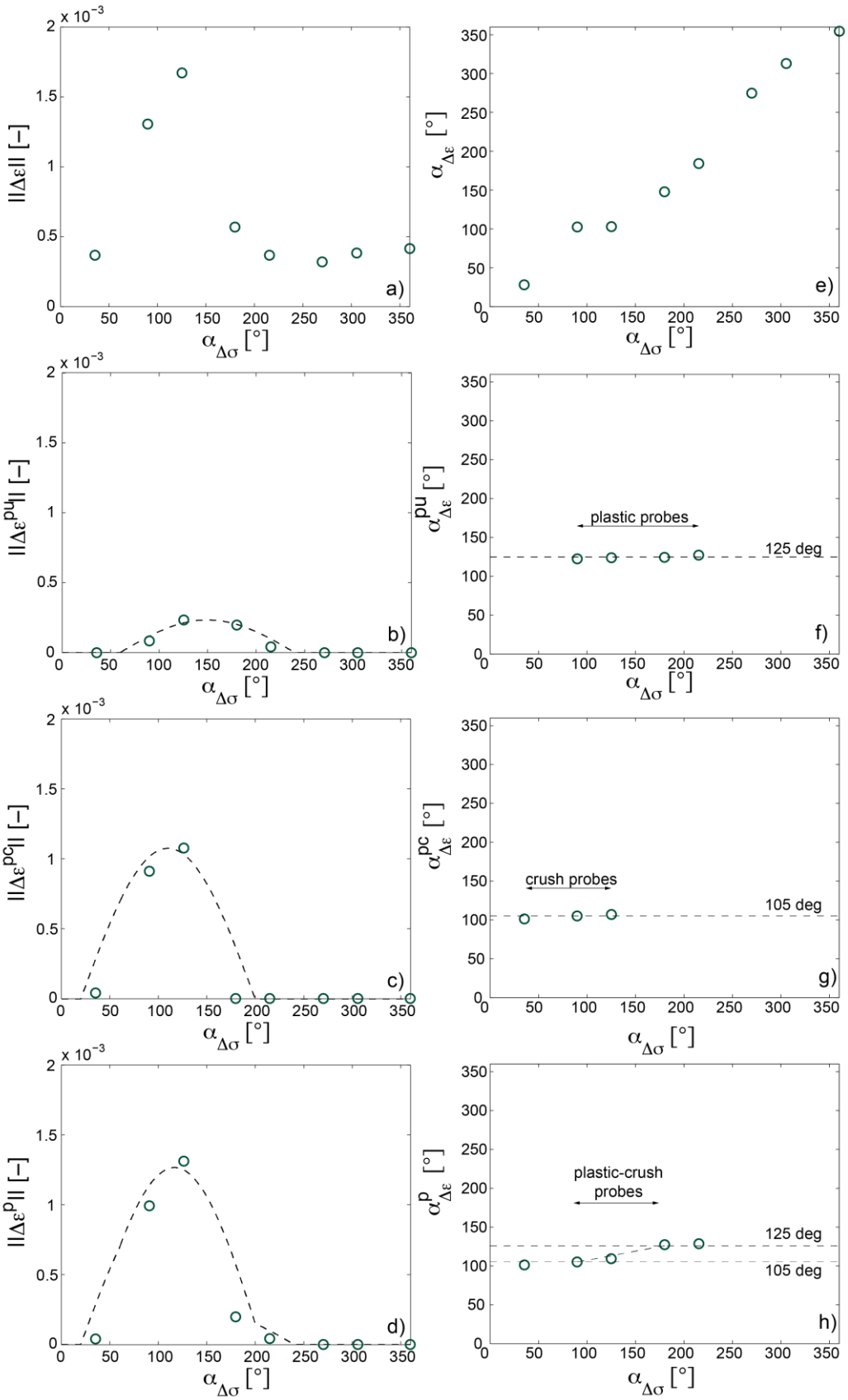

Figure 7. Total, plastic-uncrushable, plastic-crushable and complete plastic strain analysis: norm (a-d) and direction (e-h) of strain increment vectors vs. stress probe direction. Plastic strain orientation only shown for probes with significant plastic strain magnitude.

4.3 Robustness of the strain decomposition

The parallel-probe approach proposed here to separate plastic-uncrushable and plastic-crushable incremental strain contributions can be checked using several alternative procedures. One possibility is to perform two load-unload probes, one with crushing activated another without crushing. This was done for point A (Figure 8) and, at the end of the procedure (Figure 8d), the same results were obtained as with the parallel-probe approach.

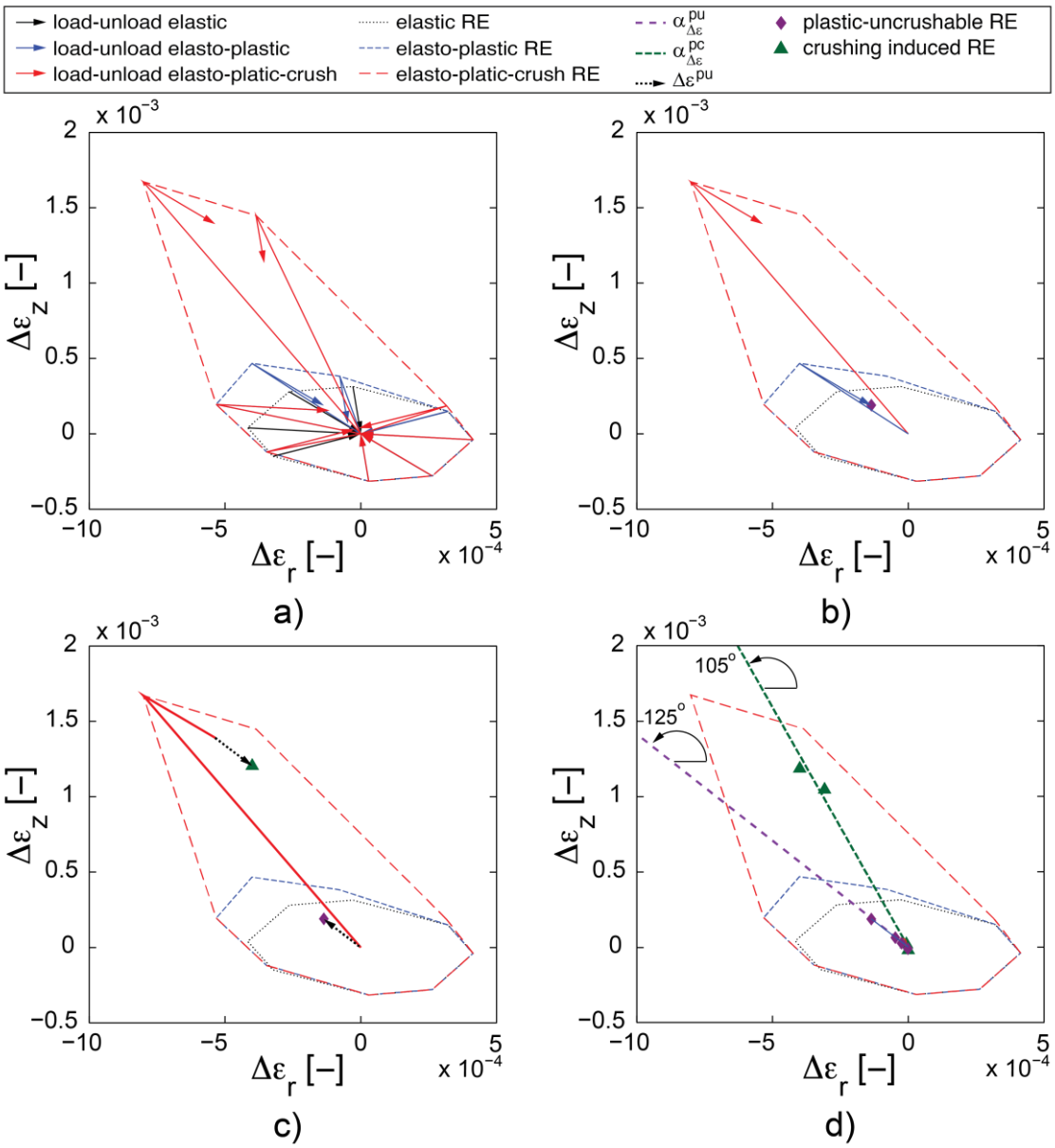

Figure 8 Obtention of the response envelope at point A by a load-unload method a) load-unload strain vectors for elastic (black) elasto-plastic-uncruahbale (blue) and elasto-plastic-crushable (red) with corresponding elastic, elasto-plastic and elasto-plastic-crush RE b) load-unload plastic crushable and uncrushable strain vectors for DC probe with the identification of the corresponding plastic-uncrushable RE point (diamond) c) determination of the crushing induced RE: subrtruction of the plastic-uncrushable vector to the load-unload strain vector for the elasto-plastic-crushable case, d) plastic and plastic-crushable incremental strains obtained using the load-unload method.

Probing from other initial states It appeared that sometimes crushing events would also occur on the incremental unload path. That complicated the comparison with the parallel-probe approach and an alternative verification method was devised, based on separate computation of a pure-crushing incremental response.

In this method,

1. A stress probe is applied to the specimen described by the reference discrete model. It provides the total strain increment $\Delta\varepsilon$
2. The same stress probe is applied to the non-crushable counterpart of the original specimen, in which crushing is inhibited. It provides the conventional elasto-plastic strain increment $\Delta\varepsilon^{ep}$
3. In a specimen described by the reference discrete model all the particles that failed in the initial probe are simultaneously broken. Stress is kept constant. The response thus observed is purely plastic –breakage is unrecoverable- and this provides the plastic strain due to crushing i.e. the plastic-crushable incremental strain $\Delta\varepsilon^{pc}$

This procedure allows direct verification of the identity in equation (15). As illustrated in Figure 9, the identity holds with a very close degree of approximation. The slight differences are probably caused by the fact that in the reference probe crushing events are not simultaneous.

Using this pure-crushing method a number of verifications were carried at different initial states and the strain-decomposition results were always very close to those obtained using the parallel probe method. This latter method is computationally more efficient and was adopted henceforth for systematic testing.

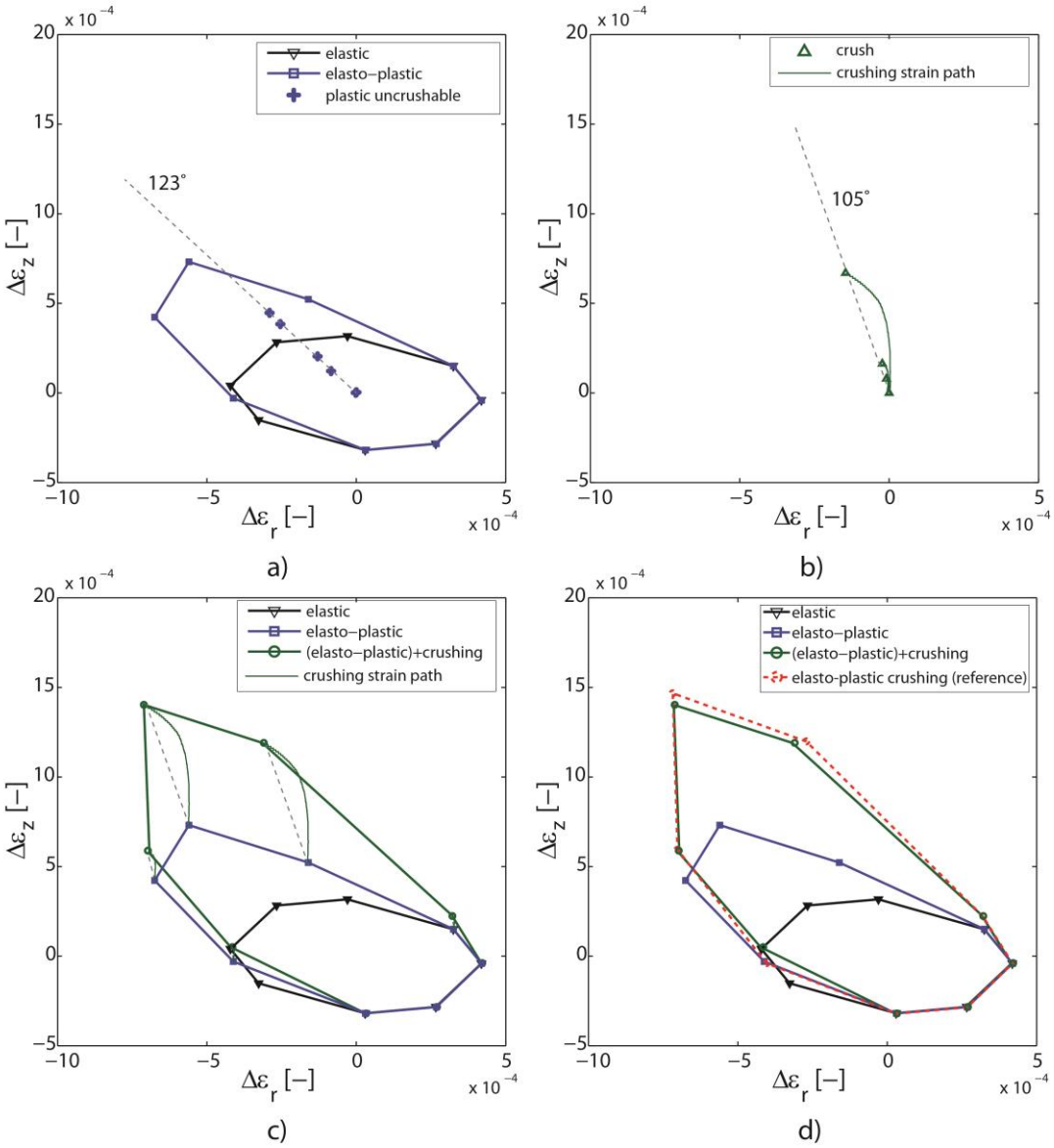

Figure 9 Plastic strain decomposition: a) elastic and elasto-plastic response envelopes, b) one example of crushing strain path c) separately computed crushing strain paths added to an elasto-plastic envelope d) comparison of the precedent with the reference elasto-plastic-crushable probe

4.4 Effect of splitting configuration on strain response envelopes

As stated above, Ciantia et al (2015) compared alternative splitting configurations, concluding that, despite the inherent mass loss, the 14-ball crushed configuration represented in Figure 1 resulted in the same macroscopic behavior obtained with more numerous splitting configurations. An example of this kind of result for an oedometric path is shown in Figure 10.

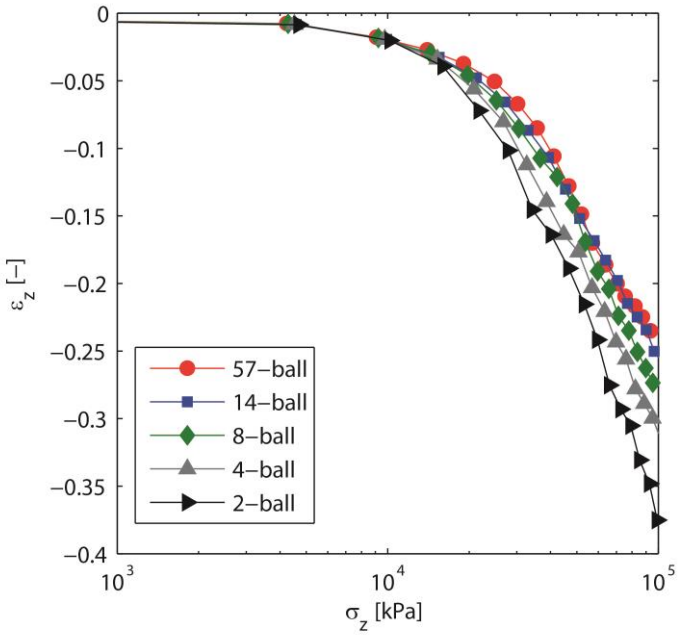

Figure 10 Effect of splitting configuration choice on the oedometric response of a granular material

Incremental probing obviously results in much less crushing and mass loss than that appearing on a whole test. It seemed likely that the same splitting configuration would work as well for incremental paths. As a check, the strain response envelope at point A was re-evaluated using three sets of parallel simulations: one in which every broken particle was completely deleted (particle mass loss 100%); a second using the preferred 14 particle split (particle mass loss 47%) and finally a third in which instead a 57 particle split was used (particle mass loss 37%). As shown in Figure 11, the response envelopes obtained in the three cases were practically identical. This confirms that the extra volumetric strain appearing upon crushing is not caused by mass loss, but rather by post-breakage rearrangement (crushing induced plastic deformation).

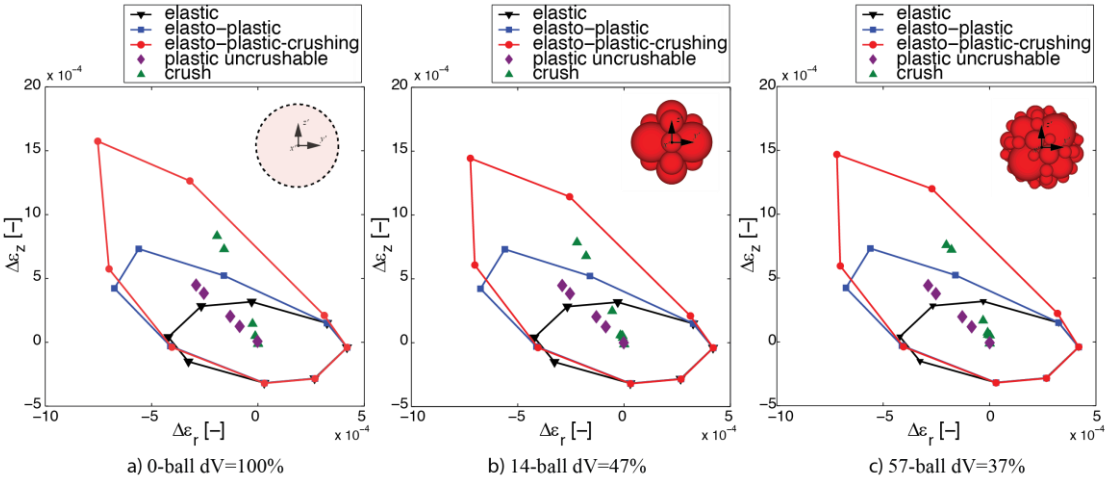

Figure 11 Strain response envelope at point A on the oedometric path evaluated with different post-beakage assumptions a) complete particle deletion, b) 14 particle split and c) 57 particle split.

This result is not surprising because the amount of mass lost in these incremental probes is minimal. Table 3 reports the maximum % of deleted mass in the simulations presented in the paper (with a 14-particle split) as well as what would have resulted using the alternative splits. It was thought that 0.1% of mass loss in a probe was a reasonable upper limit, and that gave another reason why the small REV model was discarded.

Table 3 Deleted mass during stress probe

	Small REV	Mid REV	Large REV
% Deleted mass if whole particle is deleted	0.39	0.17	0.05
% Deleted mass if 14 split configuration is used	0.18	0.08	0.02
% Deleted mass if 57 split configuration is used	0.07	0.03	0.01

4.5 Spatio-temporal localization

Results of incremental probing will be difficult to interpret if crushing events would gather in a particular spatial zone of the specimen. For instance, cemented DEM specimens had been shown to form localized compaction bands when crushing was simulated using a similar method (Marketos & Bolton, 2009).The spatial localization of crushing events was then examined for a number of probes. Crushing events did not show any clear localization pattern, as shown in Figure 12 illustrating a typical result. These results are similar to those observed by Esnault & Roux (2013), who went on to note that although crushing events were not localized in space they were typically grouped in time, or in their words, had a *cascading nature*.

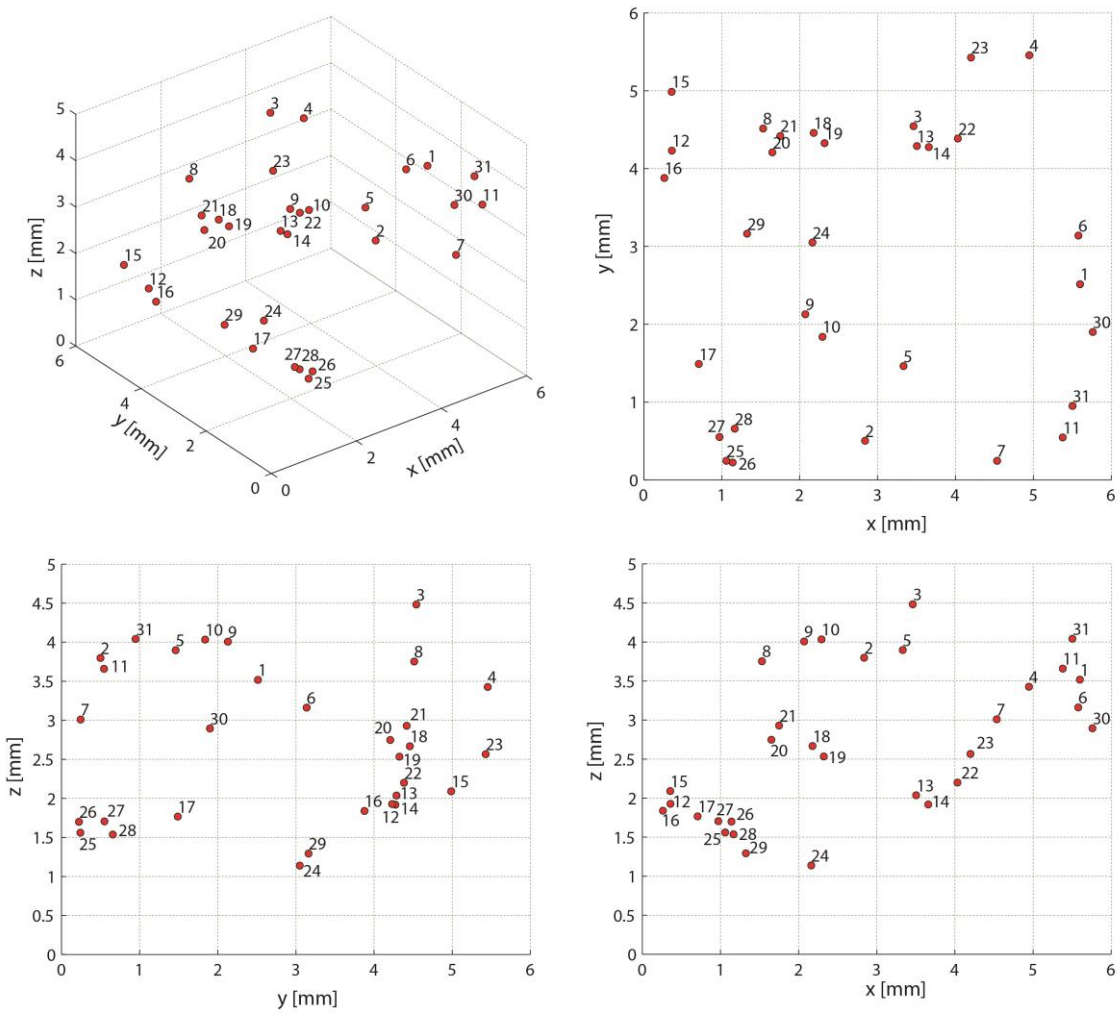

Figure 12. Spatial disposition (perspective and coordinate plane projections) and order of crushing events for a probe alongside DC on large sized sample. Numbers indicate the crushing sequence.

Indeed, that cascading nature was also visible here. Particularly important symptoms of this were stress oscillations that appeared upon probing (Figure 13). Particle crushing induces a local dynamic instability in the granular network that complicates stress path control. In some cases the time-clustering of crushing events might overcome the capacity of the servo control to maintain the target stress path. The imposed stress probe magnitude is then unclear and the validity of the response envelope obtained may be questioned.

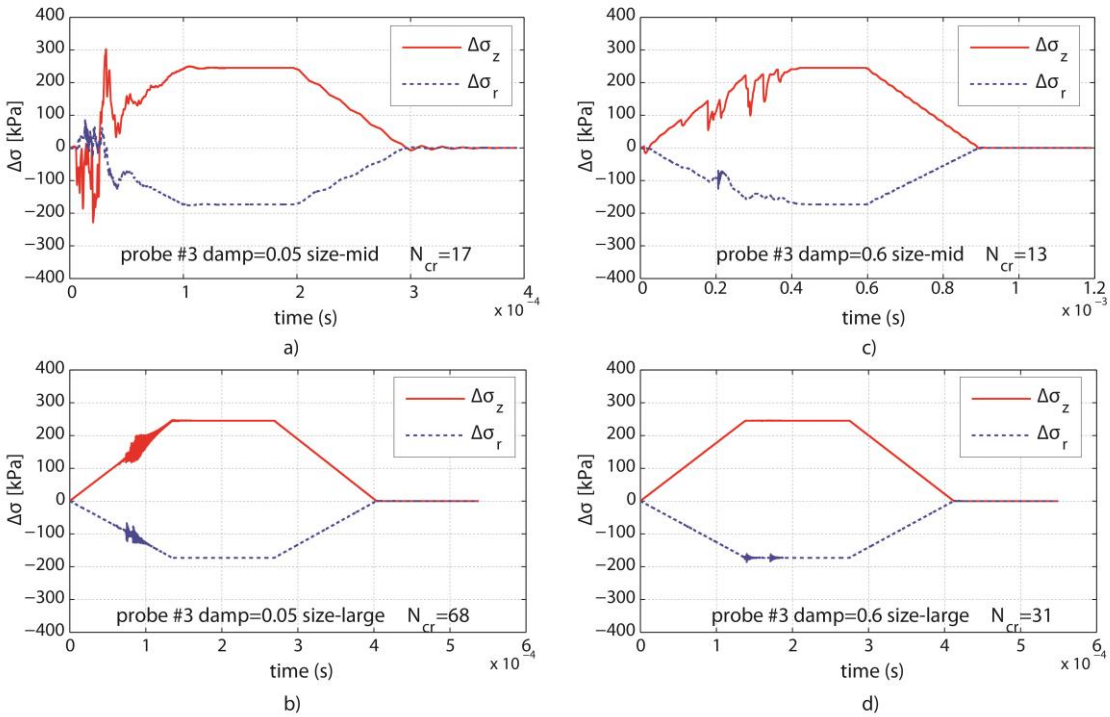

Figure 13. Stress history imposed on the sample for DC probe at point A in the case of: a) medium-sized sample and low damping (0.05), b) large-sized sample and low damping (0.05), c) medium-sized sample and high damping (0.6) d) large-sized sample and high damping (0.6). N_{cr}: number of crushing events during the probe.

Initial exploration of this phenomenon showed that it was clearly influenced by specimen size. Dynamic instability was more intense in the medium sized specimen (Figure 13a, c) that in the larger sized one, (Figure 13 b,d), despite the fact that the number of breakage events was smaller in the former case. A likely explanation is that a larger number of particles does imply a more redundant force network to carry the applied stress from one wall to its opposite.

Increasing specimen size to achieve dynamical smoothing is inconvenient because of a significantly increased computational cost and alternatives were sought. Alternative strategies to reduce instability may include, for instance, improved stress-wall control algorithms or introducing fluid coupling on the simulation (Climent et al. 2013). The simplest one, however is to increase damping. Indeed, as shown in Figure 13, increased damping resulted in much reduced dynamic instability –compare panels a and b in Figure 13, with panels c and d.

A non-viscous local damping, δ, (Cundall, 1987) is used here. A sensitivity study to the value of this parameter was performed. Increasing damping in a stress probe reduces the number of crushing events and the magnitude of plastic-crushable strain (Figure 14). Above a certain damping threshold, both crushing events and $\Delta\varepsilon^{pc}$ magnitude stabilize. The orientation of incremental crushing strains is insensitive to damping (Figure 14f). Damping does not affect the magnitude or orientation of the plastic-uncrushable component (Figure 14b, 6e).

In a case in which parallel experimental results are available the numerical damping level may be calibrated to recover the observed incremental strain magnitude. Here the value of local damping was chosen for pragmatic reasons, as a large value (0.6) so that the systematic stress-probing presented later could be performed using the medium-size specimen as REV.

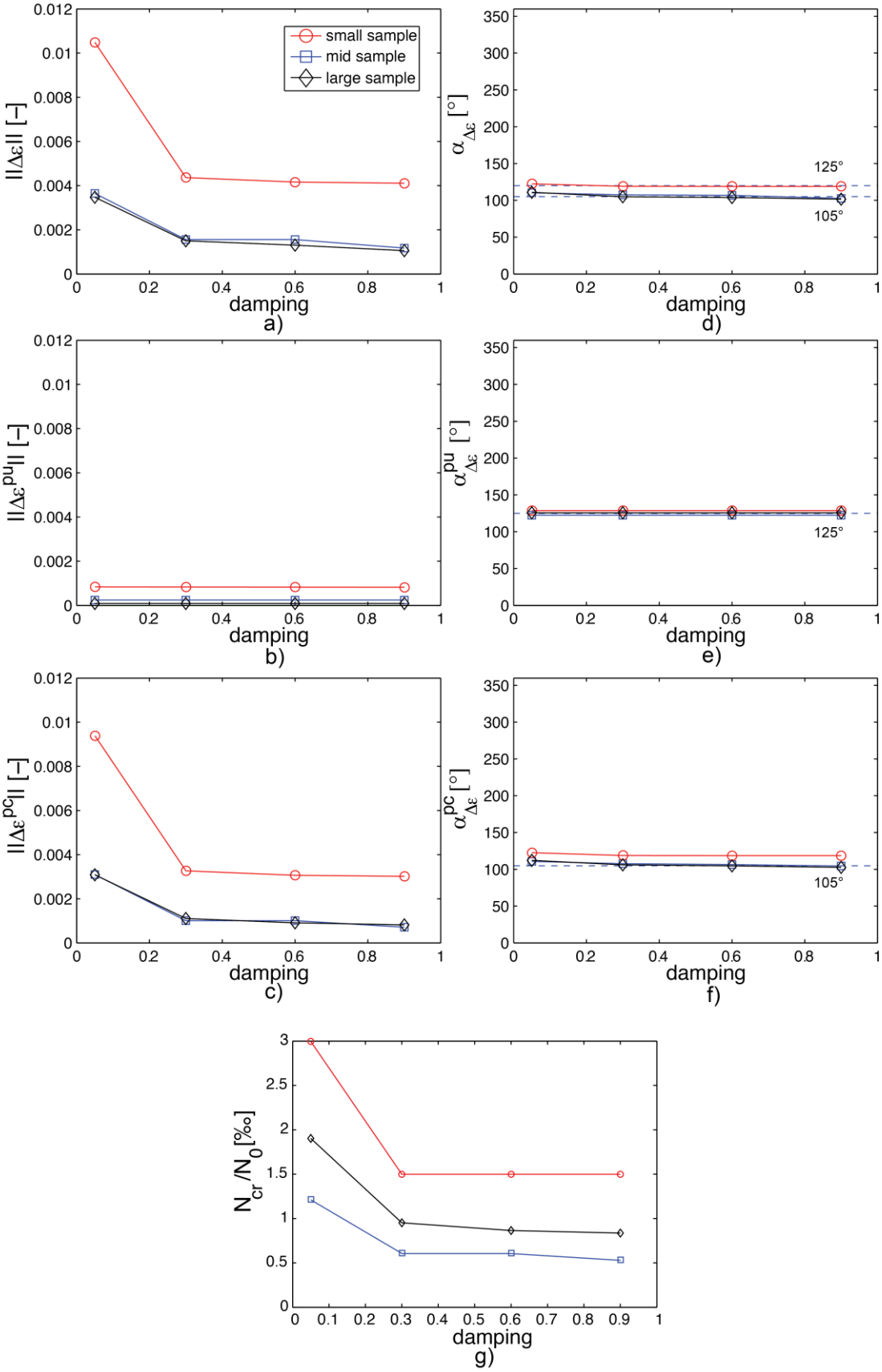

Figure 14 Effect of damping on incremental strain magnitude and orientation for DC probe at point A: Magnitude of total, plastic-uncrushable and plastic-crush strains as function of damping (a-c) and corresponding strain orientation (d-f). g) Effect of damping on number of crushing events for DC probe.

5 Incremental strain response on the triaxial plane

5.1 The effect of OCR: oedometric case

In this section the effect of over consolidation ratio (OCR) on the incremental response of the material is investigated. Three points alongside an oedometric path (Figure 5c) have been selected for investigation. In particular, the response envelope at point B (σ_z = 50 MPa, OCR=1) and point C (σ_z= 31.5 MPa OCR=1.59) are compared with that at point A (σ_z = 31.5 MPa OCR=1).

Figure 15a compares the GSD for the three initial stress states. Clearly, increasing the load from point A to B causes the GSD to evolve increasing the % of fines. On the other hand, the GSD remains unchanged upon unloading (going from B to C). Indeed no particle crushing was recorded during the unloading phase.

The results of the stress probes performed at these three distinct initial conditions are reported in Figure 15b-d where the elastic, elasto-plastic and elasto-plastic + crush RE for points A, B and C are drawn. Comparing the responses at points A & B it appears that continuous oedometric loading has resulted in incremental hardening. The amount of incremental plastic strain recorded at B is far smaller than that at A. That reduction is mostly due to the crushable component, which is very much diminished in going from A to B.

At the over-consolidated state (point C) no crushing is observed for any stress probing direction. On the other hand the material develops plastic deformations for probing directions that are diametrically opposite to the ones inducing irreversible deformations in the normally consolidated state at the same stress level (point A). The existence of incremental plastic strains at pre-loaded states had been previously noted by Calvetti et al (2003).

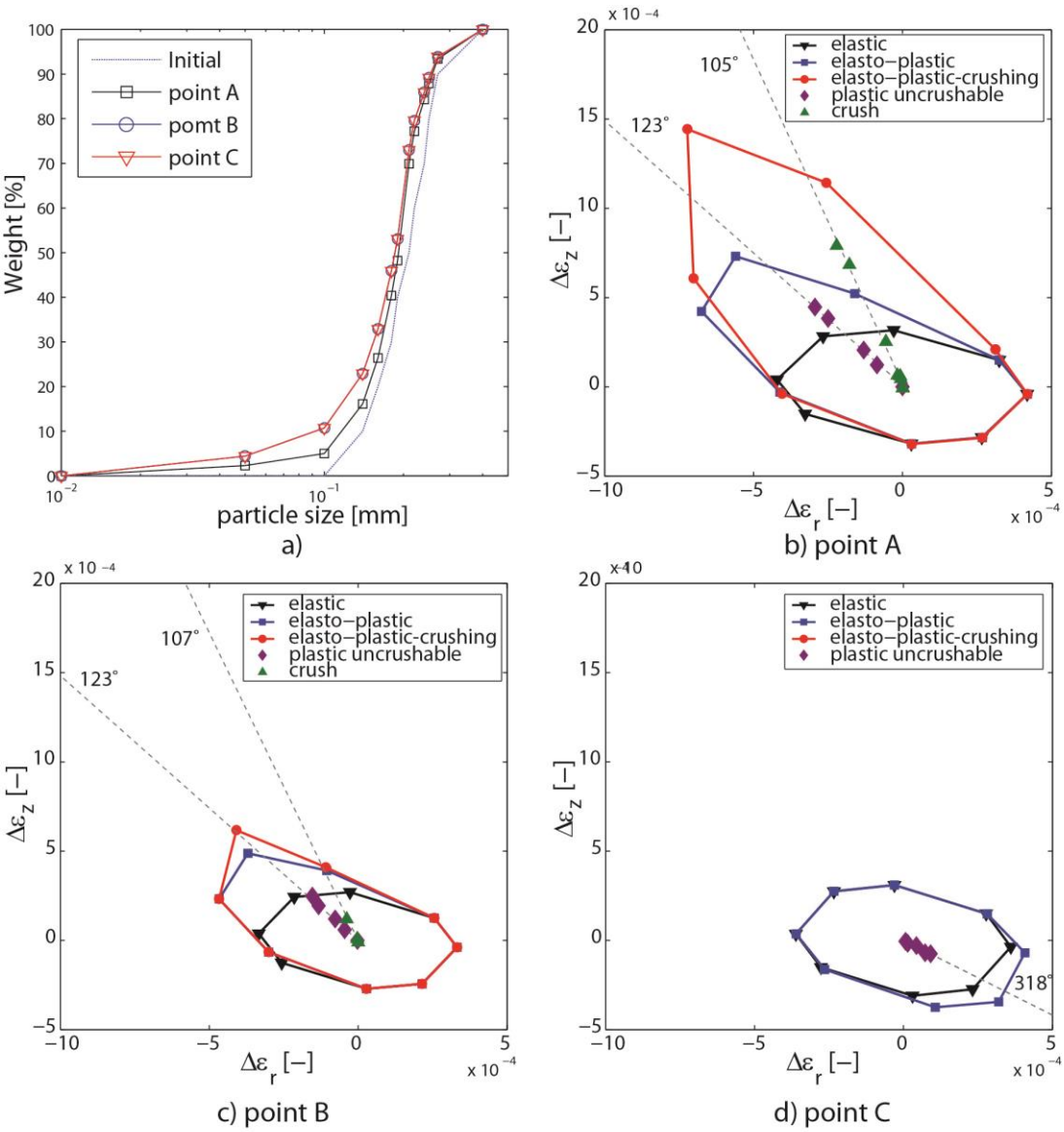

Figure 15 a) GSD of the medium sample at points A, B and C, b-d) response envelopes at points A, B and C respectively.

5.2 Effect of stress ratio and grading index

In this section response envelopes were obtained at 12 distinct stress states in the triaxial plane. The initial conditions lay on radial compression stress paths, in which the numerical sample was continuously loaded at a fixed stress ratio (η = q/p') of either 0 (isotropic), 0.3, 0.75 and 1. During these radial stress paths the specimen GSD evolution was tracked and the grading index computed.

Figure 16a shows the radial compression stress paths in the triaxial plane and the 12 initial conditions selected for incremental testing. On Figure 16b the grading index evolution of the same numerical tests is plotted as a function of the mean effective stress. It may be noted that the sigmoidal shape that described I_G evolution is very similar to that observed in previous experimental work on crushable soils (Coop et al 1993; Vilhar et al. 2013). Despite this

encouraging similitude, it is beyond the scope of the present work to further explore factors affecting I_G evolution (e.g. stress path, model parameters…). The focus instead is on incremental responses, and tracking I_G is useful so that conditions with the same degree of GSD evolution can be selected alongside the different stress paths. As indicated in Figure 16b the I_G levels selected for analysis correspond to different stages of the GSD evolution.

A summary of the initial conditions selected for incremental testing is given in Table 4. The stress increment magnitude for each probing point, also reported in Table 3, was obtained as 1% of the maximum principal stress of the initial condition.

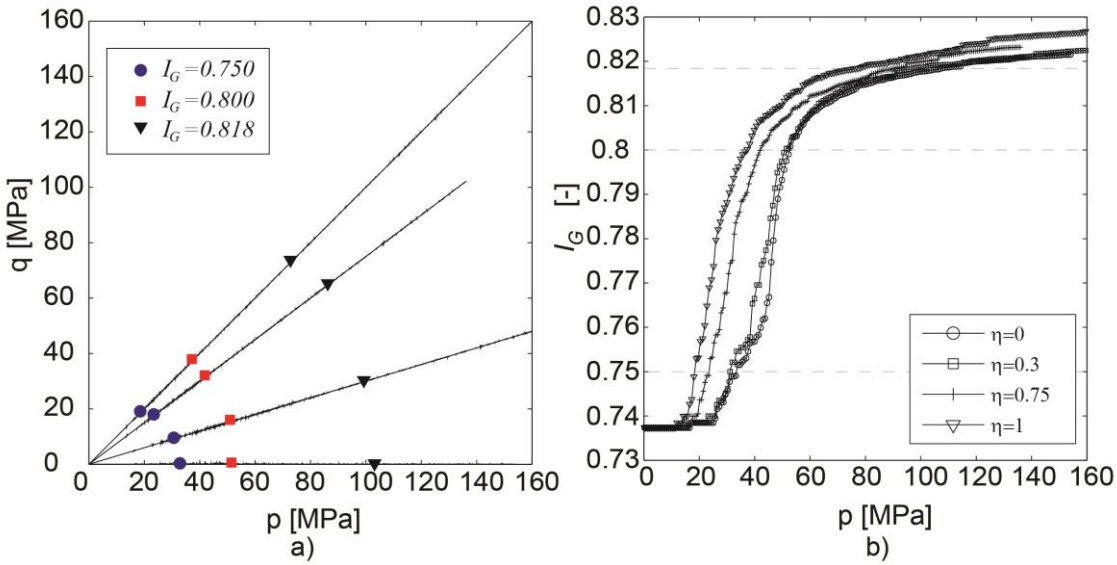

Figure 16 a) Radial stress paths indicating initial conditions for response envelope evaluation b) I_G evolution during radial stress paths; horizontal lines indicate the levels selected for stress probing.

Table 4. Initial conditions for iso-I_G stress probes in triaxial plane

Stress path	*Test ID*	I_G	*p [kPa]*	*q [kPa]*	$\Delta\sigma$*[kPa]*	N_i
η=0	A0	0.75	33175	0	332	10618
	B0	0.8	52183	0	522	24736
	C0	0.818	103770	0	1038	42130
η=0.3	A03	0.75	31083	9325	373	10644
	B03	0.8	51456	15437	617	25568
	C03	0.818	100000	30000	1200	40115
η=0.75	A075	0.75	23387	17540	351	10696
	B075	0.8	41964	31473	629	26075
	C075	0.818	86579	64934	1299	41155
η=1	A1	0.75	18500	18500	308	10748
	B1	0.8	37311	37311	622	26205
	C1	0.818	72915	72915	1215	41896

The main results of this probing campaign are presented in Figure 17 to Figure 21. Figure 17 presents at the 12 initial states the total (elasto-plastic-crushing), elasto-plastic (no crush), and

elastic response envelopes. Each panel in Figure 17 also includes the two incremental plastic strain components, uncrushable and crush.

The elastic RE have an elliptic shape, and are centered at the origin of the strain increment space. As the stress ratio increases from η=0 to η=1, the elastic response envelope becomes larger and more elongated while presenting a slightly anticlockwise rotation. On the other hand, for a fixed stress ratio η increasing grading evolution (hence higher mean stress) does not seem to affect the elastic RE.

For the more isotropic stress ratios η=0 and 0.3 plastic-uncrushable strains are very small and elasto-plastic RE practically coincide with the elastic ones. Increased deviatoric conditions (η=0.75 and η=0.1) result in much increased plastic-uncrushable incremental strains. This is in agreement with observations made by Calvetti et al 2003 when probing uncrushable specimens at smaller stress levels.

Plastic-crushable incremental strains appear instead at all deviatoric stress levels. They appear to decrease with increased IG. Both components of plastic strain appear always aligned in one direction, with the crushable component direction always found clockwise from the uncrushable one (i.e. having a larger volumetric component).

A clearer view of the incremental plastic strains obtained at each probing point is given in Figure 18 to Figure 21. Magnitude and orientation of each incremental plastic strain component as well as their sum, the total plastic strain, are presented as a function of stress probe orientation. Examining these figures several observations can be made:

1) At every probing point each separate plastic strain component (crushable and uncrushable) always has a well-defined flow direction. These directions (panels a, b) are not affected by IG (i.e. by GSD evolution).
2) For both plastic flow components the direction of plastic flow rotates clockwise (i.e. becoming more deviatoric) as η increases. Whenever both the components appear the plastic-uncrushable one is always more deviatoric than that due to crushing, (compare panels a & b)
3) There is no simple pattern as to which incremental plastic strain component is larger, except at isotropic conditions where all the plastic strains are due to crushing. At the other deviatoric stress levels the relative magnitude of both components (compare panels d & e) varies with IG and stress probe orientation.
4) Because of those changes in relative magnitude of the incremental plastic strain components, the resultant total plastic strain flow direction may vary with stress probe direction. This is particularly visible in Figure 19c & Figure 20c.

5) The effect of IG on incremental plastic strain is systematic for the uncrushable component. The magnitude of this plastic strain component always increases as IG increases (panels d).
6) The effect of IG on the crush incremental plastic strain component is less clear. At η=0 and η=0.75 the magnitude decreases with increased IG; but this is not the case at other η values.
7) As stress obliquity increases the effect of probing direction on crushable component magnitude (panels e) becomes closer to that of the uncrushable component (panels d)
8) For the uncrushable component stress probe directions causing larger strains –i.e. with smaller tangent stiffness- are further away from the stress path direction than for the crushable component.

Finally in Figure 22 the direction of plastic flow is represented in the deviatoric plane for the 12 initial conditions analyzed in this section. Directions for each component are always well defined, whereas for the total incremental plastic strain sometimes not (i.e. they can vary within the sector indicated, depending on incremental stress probe direction). It is clear from this representation that, except at the largest stress obliquity, the crushable component of flow is better aligned with the previous stress path than the uncrushable component, always more deviatoric.

.

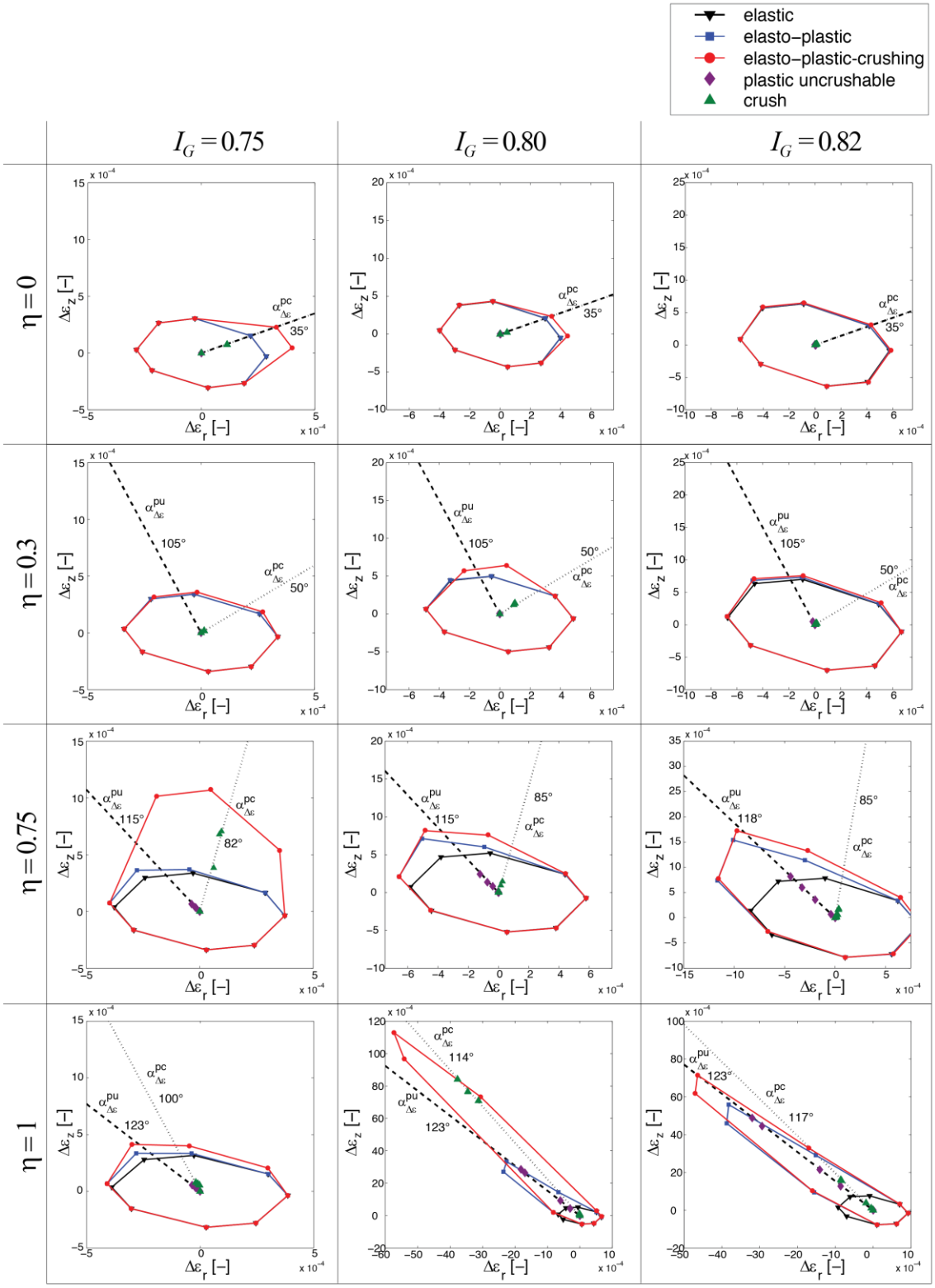

Figure 17 Response envelopes for the 12 initial conditions considered. Each row corresponds to a different radial loading path (from top to bottom n=0, 0.3, 0.75 and 1, respectively) and each column corresponds to a grading index level.

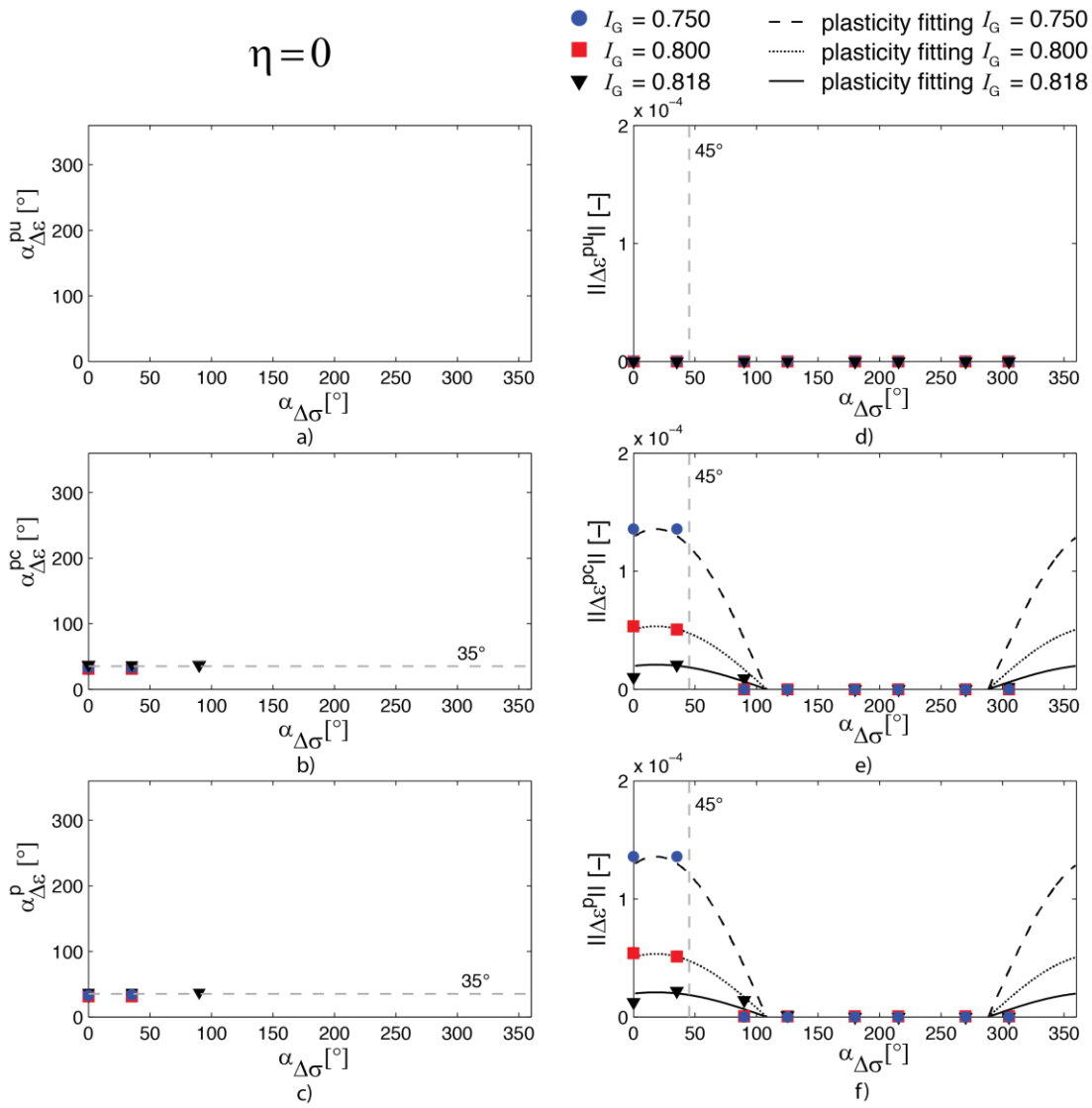

Figure 18 Plastic flow analysis for η=0; a-c) plastic flow direction and (d-f) norm of plastic deformation as a function of loading direction. The loading direction is at 45 degrees

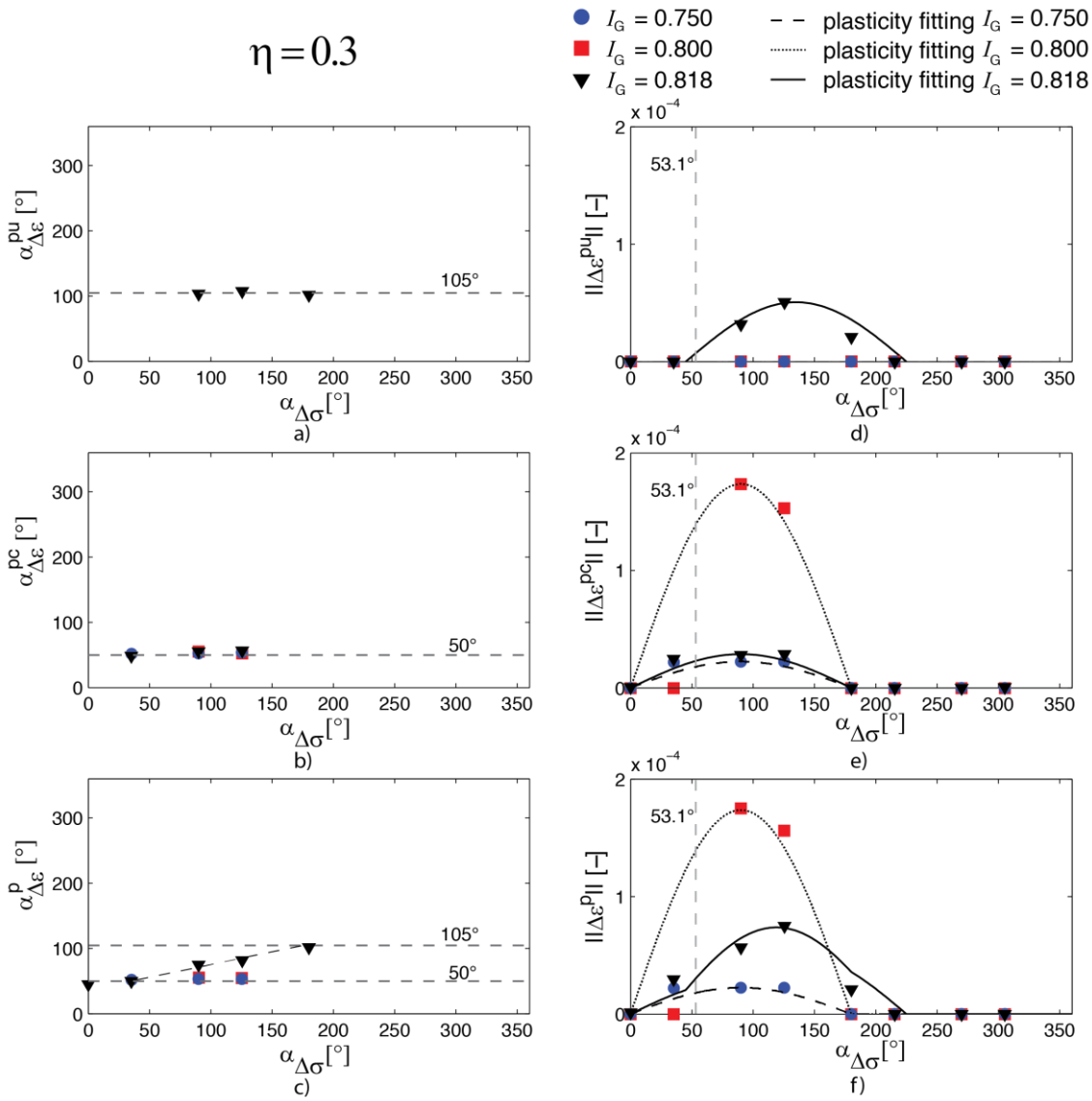

Figure 19 Plastic flow analysis for η=0.3; a-c) plastic flow direction and (d-f) norm of plastic deformation as a function of loading direction. The loading direction is at 53 degrees

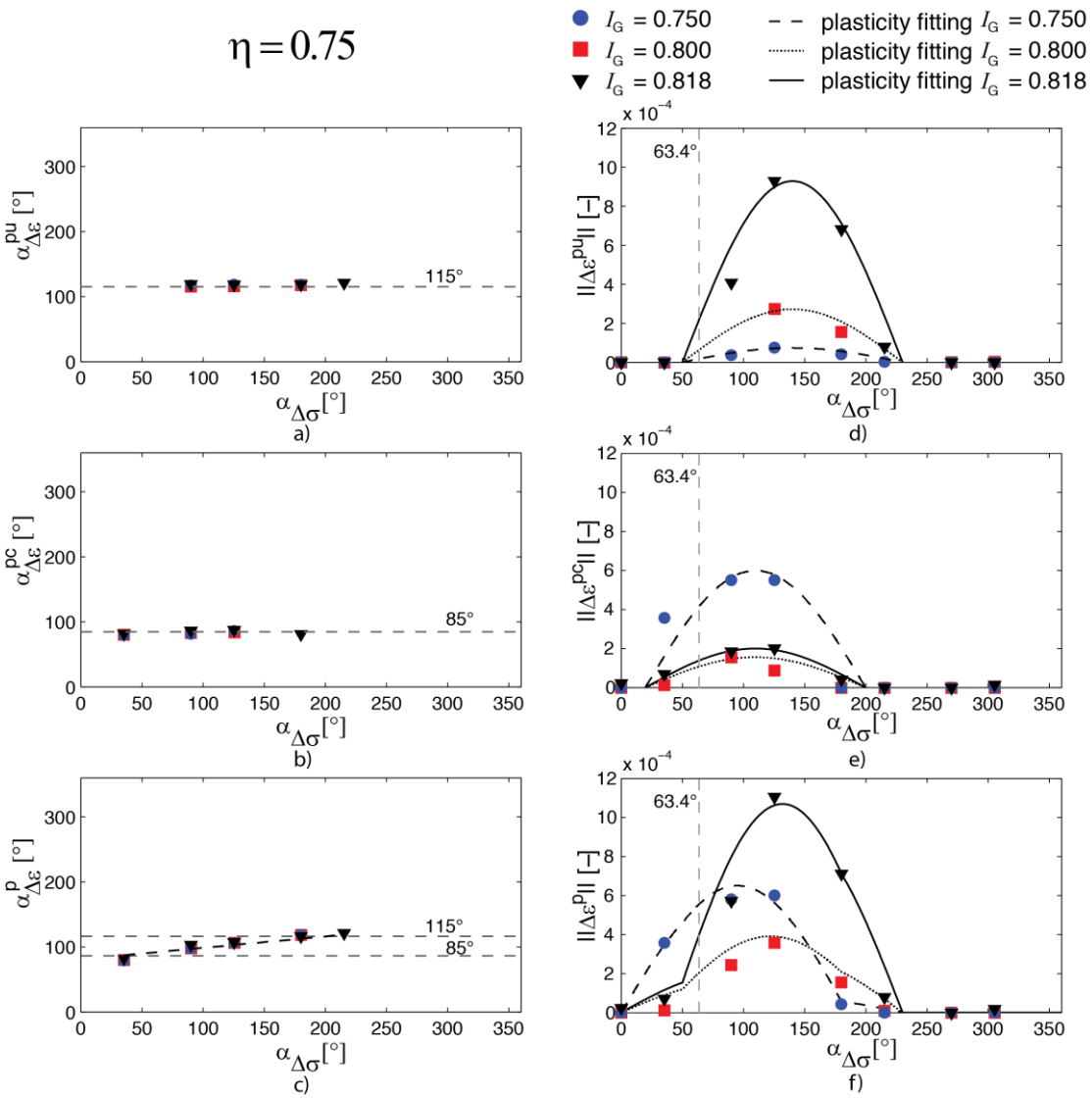

Figure 20 Plastic flow analysis for η=0.75; a-c) plastic flow direction and (d-f) norm of plastic deformation as a function of loading direction. The loading direction is at 63 degrees

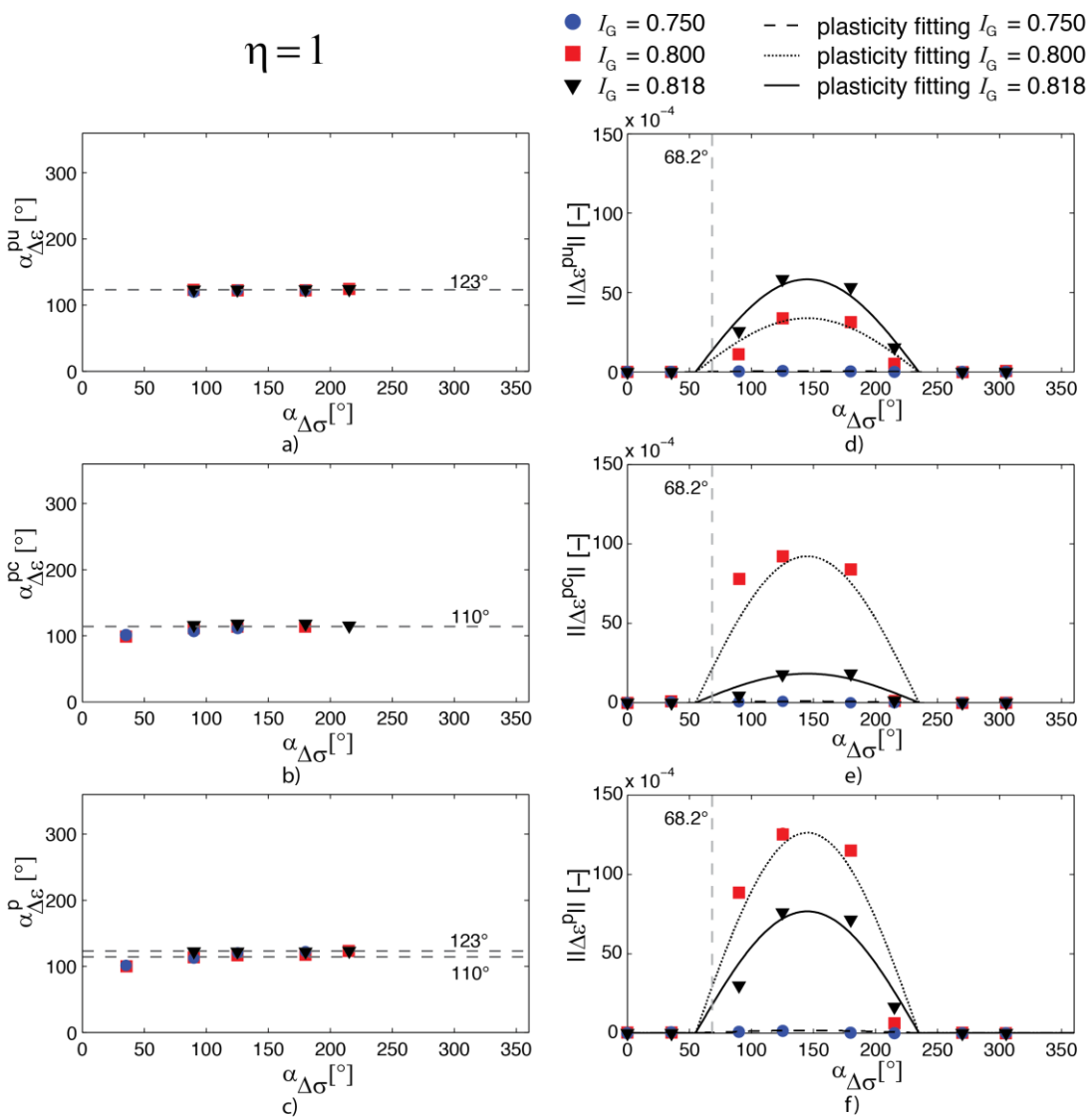

Figure 21 Plastic flow analysis for η=1; a-c) plastic flow direction and (d-f) norm of plastic deformation as a function of loading direction. The loading direction is at 68 degrees

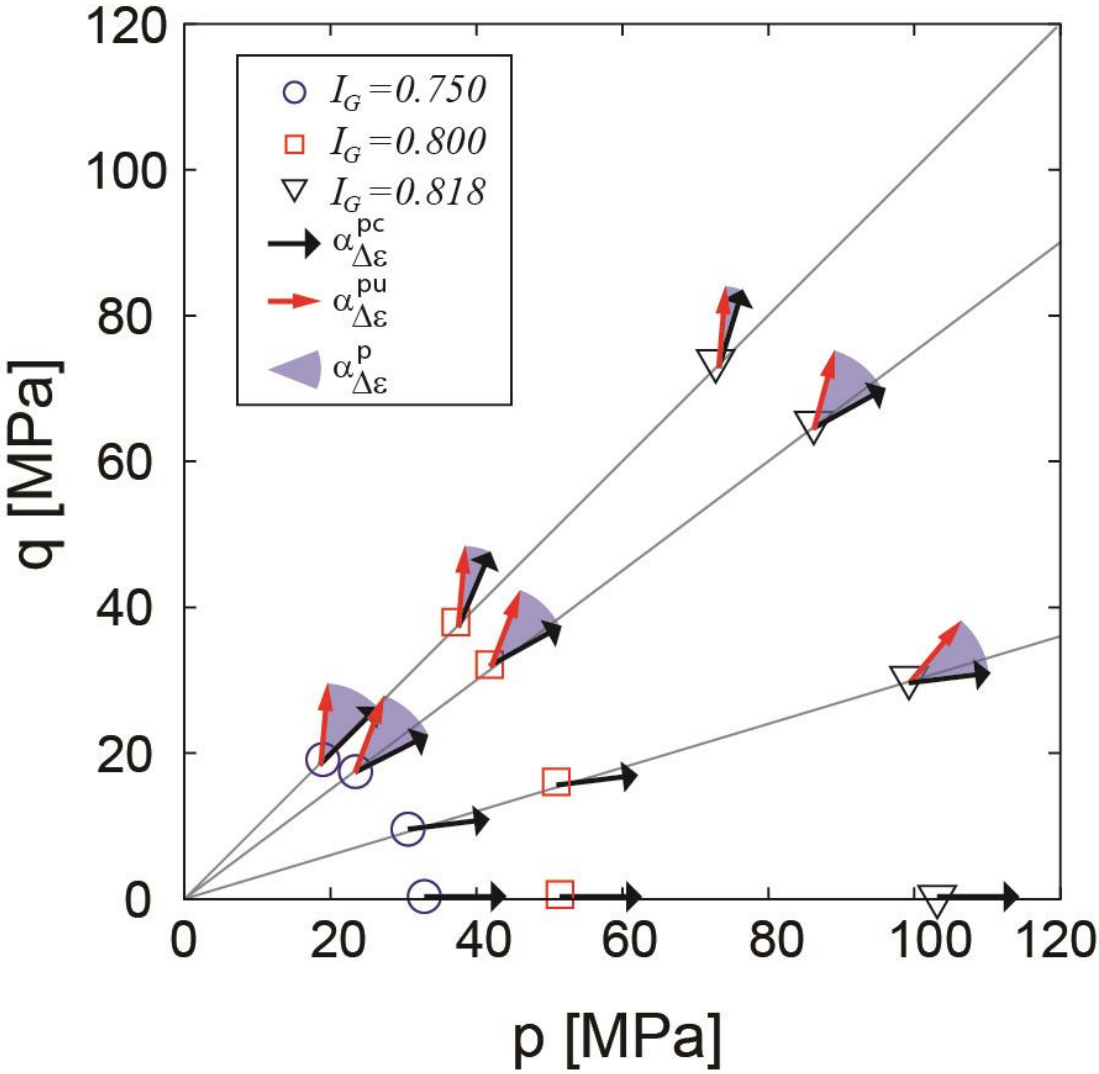

Figure 22. Plastic flow direction: No crush, only crush and plastic+crush.

5. Concluding remarks

A new procedure has been proposed to obtain incremental responses of DEM analogues of crushable soils. The robustness of the method has been discussed in detail. Its potential has only being indicated by a few examples.

A direct experimental verification of the parallel probe approach would be desirable. It is perhaps worth speculating, how that may be arranged. A possible scenario would include, for instance, an artificial highly crushable soil (e.g. LECA, Casini et al. 2013) tested with and without some crushing-inhibiting coating. Until that or other procedure is applied, experimental support for the proposed method would have to be obtained by matching responses of crushable materials on different scenarios (e.g. Ciantia et al (2015); Ciantia et al. (2014b)).

No attempt has been made to evaluate the energy balance of the probes. This is certainly a subject worth of future research, for instance by evaluating energy efficiency (Esnault & Roux, 2013) alongside different loading paths.

A large variety of continuum models have been proposed for crushable granular materials: based on single-mechanism elasto-plasticity (Cecconi et al. 2002; Liu et al. 2013), multi-mechanism plasticity (Daouadji & Hicher, 2010; Kikumoto et al. 2010), generalized plasticity (Liu & Zhou, 2012) or hypoplasticity (Engin et al 2014). Although the observations made in the probing campaign described above are perhaps easier to synthetize using multimechanism plasticity, the purpose of this contribution was not to endorse one particular constitutive approach.

Indeed, despite their different conceptual framework, all these models share one characteristic: plastic irreversible strains are modified in magnitude and tensorial direction –i.e. proportion between tensorial components- when crushing is considered. With an appropriate choice of parameters, crushing can be also suppressed in these continuum models. Therefore all these models can produce response envelopes with and without crushing, regardless of how explicit are in their statements about the plastic flow modifications due to crushing. Because all of them have this capability, a systematic exploration of the triaxial and/or deviatoric planes using DEM simulations such as those described here seems worthwhile.

Acknowledgements

This work has been supported by the Ministry of Science and Innovation of Spain through the research grant BIA2011-27217.

References

Anderson, W. F., and Fair, P. 2008. Behaviour of railroad ballast under monotonic and cyclic loading. Journal of Geotechnical and Geoenvironmental Engineering, ASCE, 134(3): 316-327

Bardet J.P. (1994), Numerical simulations of the incremental responses of idealized granular materials, *Int. J. of Plasticity*, **10**, n. 8, 879-908.

Calvetti F., di Prisco C. (1993), Fabric evolution of granular materials: a numerical approach, *Proc. First Forum Young European Researchers, Liège*, 115-120.

Calvetti, F., Viggiani, G., & Tamagnini, C. (2003). A numerical investigation of the incremental behavior of granular soils. *Rivista Italiana di Geotecnica*, *37*(3), 11-29.

Calvetti F., Viggiani G. and Tamagnini C. (2003), Micromechanical inspection of constitutive modelling. In: C. Viggiani (ed.), Constitutive Modelling and Analysis of Boundary Value Problems in Geotechnical Engineering.Benevento: Hevelius pp. 187–216.

Casini, F., Viggiani, G. M., & Springman, S. M. (2013). Breakage of an artificial crushable material under loading. Granular matter, 15(5), 661-673.

Cecconi, M., DeSimone, A., Tamagnini, C., & MB Viggiani, G. (2002). A constitutive model for granular materials with grain crushing and its application to a pyroclastic soil. International journal for numerical and analytical methods in geomechanics, 26(15), 1531-1560.

Cheng, Y. P., Bolton, M. D., & Nakata, Y. (2004). Crushing and plastic deformation of soils simulated using DEM. Geotechnique, 54(2), 131-141.

Climent, N., Arroyo, M., O'Sullivan, C., & Gens, A. (2013). Sensitivity to damping in sand production DEM-CFD coupled simulations. In POWDERS AND GRAINS 2013: Proceedings of the 7th International Conference on Micromechanics of Granular Media (Vol. 1542, No. 1, pp. 1170-1173). AIP Publishing.

Ciantia, M. O., Arroyo, M., Calvetti, F., & Gens, A. (2015). An approach to enhance efficiency of DEM modelling of soils with crushable grains. Géotechnique, 65(2), 91-110.

Ciantia, M., Arroyo, M., Gens, A. & Calvetti, F. (2014a) Particle failure in DEM models of crushable soil response NUMGE 2014, 8th Conference on Numerical Methods in Geotechnical Engineering in Delft, The Netherlands, 18-20 June 2014

Ciantia, M., Arroyo, M., Butlanska, J. & Gens, A. (2014b) DEM modelling of a double-porosity crushable granular material, International Symposium from Micro to Macro, Cambridge 2014 Taylor & Francis, 1153-1158

Coop, M. R., & Lee, I. K. (1993). The behaviour of granular soils at elevated stresses. Predictive soil mechanics Edited by GT Houlsby and AN Schofield. Thomas Telford, London, UK, 186-199

Costanzo, D., Viggiani, G., & Tamagnini, C. (2006). Directional response of a reconstituted fine-grained soil—Part I: experimental investigation. International journal for numerical and analytical methods in geomechanics, 30(13), 1283-1301.

Cundall, P.A. (1987) Distinct Element Models of Rock and Soil Structure. In Analytical and Computational Methods in Engineering Rock Mechanics, chapter 4, pages 129–163. Allen & Unwin,

Darve, F., & Nicot, F. (2005). On flow rule in granular media: phenomenological and multi-scale views (Part II). *International journal for numerical and analytical methods in geomechanics*, *29*(14), 1411-1432.

Darve, F., & Nicot, F. (2005). On incremental non-linearity in granular media: phenomenological and multi-scale views (Part I). *International journal for numerical and analytical methods in geomechanics*, *29*(14), 1387-1409.

Daouadji, A. , & Hicher, P. V. (2010). “An enhanced constitutive model for crushable granular materials.” Int. J. Numer. Anal. Methods Geomech. , 34 (6), 555–580.

Einav, I. (2007). Breakage mechanics—Part II: Modelling granular materials. Journal of the Mechanics and Physics of Solids, 55(6), 1298-1320.

Esnault, V. P. B., & Roux, J. N. (2013). 3D numerical simulation study of quasistatic grinding process on a model granular material. Mechanics of Materials, 66, 88-109.

Engin, H. K., Jostad, H. P., & Rohe, A. (2014). On the modelling of grain crushing in hypoplasticity. NUMGE 2014, 8th Conference on Numerical Methods in Geotechnical Engineering in Delft, The Netherlands, 18-20 June 2014.

Froiio, F., & Roux, J. N. (2010). Incremental response of a model granular material by stress probing with DEM simulations. In IUTAM-ISIMM Symposium on mathematical modeling and physical instances of granular flow (Vol. 1227, No. 1, pp. 183-197). American Institute of Physics.

Gudehus G. A comparison of some constitutive laws for soils under radially symmetric loading and unloading. In 3rd International Conference on Numerical Methods in Geomechanics, vol. 4, Aachen, Witte (ed.). Balkema: Rotterdam, 1979; 1309–1324.

Indraratna, B., Salim, W., & Rujikiatkamjorn, C. (2011). Advanced rail geotechnology-ballasted track. CRC Press

Jiang, M. J., Harris, D., & Zhu, H. H. (2007). Future continuum models for granular materials in penetration analyses. Granular Matter, 9(1-2), 97-108.

Kishino Y. (2003), On the incremental non-linearity observed in a numerical model for granular media. *Rivista Italiana di Geotecnica*, **37**, n. 3 (Special Issue on Mechanics and Physics of Granular Materials), 24-33.

Kikumoto, M., Wood, D. M., & Russell, A. (2010). Particle crushing and deformation behaviour. Soils and foundations, 50(4), 547-563.

Liu, H., & Zou, D. (2012). Associated generalized plasticity framework for modeling gravelly soils considering particle breakage. Journal of Engineering Mechanics, 139(5), 606-615.

Liu, M., Gao, Y., & Liu, H. (2013). An elastoplastic constitutive model for rockfills incorporating energy dissipation of nonlinear friction and particle breakage. International Journal for Numerical and Analytical Methods in Geomechanics.

Marketos, G., & Bolton, M. D. (2009). Compaction bands simulated in discrete element models. Journal of structural Geology, 31(5), 479-490.

McDowell, G.R., & de Bono, J. P. (2013). On the micro me-chanics of one-dimensional normal compression. Géotechnique, 63(11), 895-908

Muir Wood D. The magic of sands. Canadian Geotechnical Journal 2007; 44:1329–1350.

Plassiard, J. P., Belheine, N., & Donzé, F. V. (2009). A spherical discrete element model: calibration procedure and incremental response. *Granular Matter*, *11*(5), 293-306.

Russell, A. R. & Muir Wood, D. (2009). Point load tests and strength measurments for brittle spheres. I. J. of Rock Mech. And Mining Sciences 46, 272–280

Russell, A. R., Muir Wood, D. & Kikumoto, M. (2009). Crush-ing of particles in idealised granular assemblies. J. Mech. Phys. Solids 57, No. 8, 1293–1313.

Salim W, Indraratna B. (2004) A new elastoplastic constitutive model for coarse granular aggregates incorporating particle breakage. Canadian Geotechnical Journal; 657–671

Tamagnini, C., Calvetti, F., & Viggiani, G. (2005). An assessment of plasticity theories for modeling the incrementally nonlinear behavior of granular soils. *Journal of engineering mathematics*, *52*(1-3), 265-291.

Tamagnini, C., Viggiani, G., Chambon, R., & Desrues, J. (2000). Evaluation of different strategies for the integration of hypoplastic constitutive equations: Application to the CLoE model. Mechanics of Cohesive-frictional Materials, 5(4), 263-289.

Thornton, C., & Zhang, L. (2010). On the evolution of stress and microstructure during general 3D deviatoric straining of granular media. *Geotechnique*, *60*(5), 333-341

Vilhar, G., Jovičić, V., & Coop, M. R. (2013). The role of particle breakage in the mechanics of a non-plastic silty sand. Soils and Foundations, 53(1), 91-104.

Wan, R., & Pinheiro, M. (2013). On the validity of the flow rule postulate for geomaterials. International Journal for Numerical and Analytical Methods in Geomechanics.

Yang, Z. X., Jardine, R. J., Zhu, B. T., Foray, P. & Tshua, H. C. (2010) Sand grain crushing and interface shearing during displacement pile installation in sand Géotechnique 60, No. 6, 469–482